KTH Electrical Engineering

System Aspects and Modulation Strategies of an HVDC-based Converter System for Wind Farms

Stephan Meier

Royal Institute of Technology
School of Electrical Engineering
Electrical Machines and Power Electronics

Stockholm 2009

Submitted to the School of Electrical Engineering, KTH, in partial fulfillment of the requirements for the degree of Doctor of Philosophy.

Printed in Sweden
Universitetsservice US-AB

TRITA–EE 2009:018
ISSN 1653–5146
ISBN 978–91–7415–292–0

This document was prepared using LaTeX.

Abstract

In this thesis, a new HVDC-based converter system for wind farms is investigated. It is based on a mutually commutated soft-switching converter system and provides a unique integrated solution for the wind turbine generator drive systems, the wind turbine interconnection, and the power conversion for HVDC transmission.

In a wind farm, the mutually commutated converter system is a distributed system. A medium-frequency collection grid connects the converter station, equipped with a single-phase voltage source converter and a medium-frequency transmission transformer, with the wind turbines, each containing a cycloconverter and a medium-frequency distribution transformer. In this thesis, various system aspects regarding the application of a distributed mutually commutated converter system in a wind farm are investigated. Special attention is paid to the design of a medium-frequency collection grid that has an acceptable level of transient overvoltages, the design of medium-frequency transformers with suitable magnetic, electric and thermal properties, and the development of a strategy to commutate the voltage source converter during low power generation.

In order to adapt the mutually commutated converter system for an application in a wind farm, it had to be further developped. Different carrier-based and space-vector oriented modulation methods have been investigated. It turns out that for any load angle there is a quasi-discontinuous pulse width modulation strategy that can produce the same pulse patterns as space vector modulation. In addition, a modulation strategy has been developed that allows to replace the insulated gate bipolar transistors (IGBT) in the cycloconverter with cheap, robust, and reliable fast thyristors, despite their absence of turn-off capability. The feasibility of different modulation strategies for mutually commutated converter systems has been verified on a down-scaled prototype converter system with both IGBT- and thyristor-based cycloconverters.

Finally, a feasible wind farm layout is proposed, which considerably reduces the energy generation costs for large winds farms distant to a strong grid connection point. As a consequence, the proposed solution may facilitate the establishment of remotely located wind farms.

Keywords:

Isolated AC/DC Converter, Mutual Commutation, Soft Switching, Voltage Source Converter, Cycloconverter, Modulation Strategies, Medium-Frequency Transformer, HVDC Transmission, Wind Power, Offshore Wind Farms.

Preface

The work presented in this thesis has been carried out at the Division of Electrical Machines and Power Electronics (EME), School of Electrical Engineering, Royal Institute of Technology (KTH), Stockholm, Sweden, between March 2003 and May 2009. This project was part of the wind energy research program *VindForsk* [1], administrated by *Elforsk* [2] and financed by the *Swedish Energy Agency* [3].

The research presented in this thesis has been conducted by the author himself, if not stated differently.

This thesis is organised as an extended summary of the articles published in different international conferences.

The following remarks may ease the reading of this thesis:

- This thesis and all attached papers are available for download in pdf-format at `http://www.eme.ee.kth.se`. The pdf-files offer the possibility to zoom the pictures, do a keyword search, etc.

- The author's publications are distinguished from the other references by the use of Roman numbers. They are listed in Section 1.5.

- The sequence of authors in the publications follows this approach: The first author has done the major part of the work. Co-authors have contributed with ideas, helped to achieve results and proofread the publications. The contributions of the co-authors are approximately similar. The last author is the most senior one.

- For the help of the reader, acronyms are introduced the first time they are used in this thesis. A complete list of acronyms can be found on page 79.

Acknowledgments

This PhD project has been made possible with the financial support of the *Swedish Energy Agency* via *VindForsk*, a Swedish research program for wind power.

Over the past six years, several people have been involved in this PhD project. Hereby, I kindly acknowledge them.

First of all, I would like to thank my supervisor Prof. Hans-Peter Nee for his guidance, support, enthusiasm and trust. I am also very grateful to my second supervisor, Dr. Staffan Norrga, for valuable discussions and helpful contributions throughout the project. Many thanks to Prof. Chandur Sadarangani for giving me the opportunity to start this project at EME.

This PhD project would not have been possible without the fruitful comments and suggestions as well as guidance and support from my steering group. The steering group consists of the following members: Prof. Hans-Peter Nee (KTH), Dr. Staffan Norrga (ABB/KTH), Tomas Jonsson (ABB), Dr. Philip Kjær (Vestas Wind Systems A/S), and Dr. Jan R. Svensson (ABB). I would also like to thank former steering group members Dr. Rémy Kolessar and Prof. Lennart Ängqvist.

A great inspiration during my PhD project was the industrial cooperation with ABB Corporate Research in Västerås and Vestas Wind Systems A/S in Denmark. ABB helped me in understanding and calculating the losses and power ratings of voltage source converters and generously let me use their laboratory for measuring the cable characteristics of buried sea cables. Dr. Philip Kjær from Vestas gave me a deep insight into the recent developments in the wind power industry, once even on top of a wind turbine.

The construction of the prototype converter would not have been possible without the help of Maren Kuschke, Tommy Kjellqvist and Tomas Modéer, whose efforts are gratefully acknowledged. I would also like to thank Olle Brännvall for manufacturing the mechanical parts of the prototype and Jan Timmerman as well as Mats Leksell for their help in the laboratory.

Thanks to Peter Lönn for the computer support and Eva and Emma Pettersson as well as Brigitt Högberg for the help with the administrative work.

I would like to thank everybody at EME as well as the former employees for the friendly atmosphere at EME. Keep up the special “Roebel” spirit! In this context, I would especially like to thank my former office mates Dr. Sylvain Châtelet, Dr. Karsten Kretschmar and Tekn. Lic. Nicklas Johansson for the good time we had together. I would also like to thank Associate Prof. Juliette Soulard for sharing my entrepreneurial plans.

Many thanks go to Switzerland, most of all to my parents for their never-ending support and love. A special thank to my brother Michael, key account manager of my Swiss banking account. Many thanks also to my former fellow students at ETH in Zürich, especially Damian Aegerter and Dr. Andrea Rutz.

Last but certainly not least, I would like to thank my beloved wife Florence and my son Simon for their endless love and patience during the writing of this thesis. Je vous aime tous les deux très très fort.

Stockholm, spring 2009

S. Meier

Stephan Meier

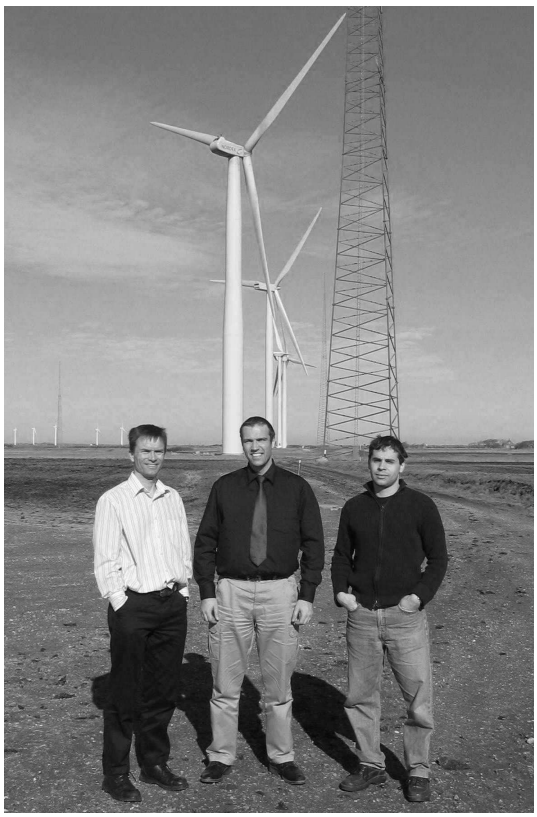

Tomas Jonsson, Hans-Peter Nee and Stephan Meier at Hœvsœre test site in Jylland, Denmark. March 2005

Contents

1 Introduction

This chapter provides the background and objectives of this project. Furthermore, the original scientific contributions of the author are presented. The outline of the thesis and the list of publications provide guidance through the content of this thesis.

1.1 Background

In 1954, the world's first commercial high-voltage direct current (HVDC) transmission system was commissioned, see Fig. 1.1 (for technical details refer to Section 2.2.1). The 100 kV, 20 MW submarine HVDC cable connects the Swedish mainland to the island of Gotland in the Baltic Sea. Ever since, HVDC transmission technology has been improving with more than 100 installations so far. Today, an emerging application area for HVDC transmission systems is the grid connection of large offshore wind farms [4]. The rapid development in wind power generation offers good chances for new concepts and technologies. This will eventually lead to

Figure 1.1: During the summer 1953, the cable of the first commercial HVDC link is drawn ashore south of Visby on the island of Gotland, Sweden (courtesy of ABB).

improvements in power quality, efficiency, reliability, and functionality, thus reducing the energy generation costs for wind power.

In recent years, the installed global wind power capacity has expanded strongly. This trend will hardly change regarding the general environmental awareness and the ambition of the European Commission to generate 12 - 14 % of EU electricity from wind by 2020 [5] (up from approximately 3.5 % in 2007). Large offshore wind farms rated at several hundred megawatts are one of the key technologies in order to achieve the energy and climate goals of the EU. At the moment, offshore wind farms are still more expensive than onshore installations. Usually, the costs for the turbine foundations grow rapidly as the water depth and wave height increases. In addition, the costs for repairs and maintenance are also significantly higher at sea. Nevertheless, locating wind farms offshore has several important advantages:

- Huge unexploited wind resources. On the contrary, profitable *onshore* locations in Europe are often already developed or in conflict with other interests.
- Less obtrusive than wind turbines on land. Projects are experiencing less resistance from NIMBYs (Not In My Back Yard) and BANANAs (Build Absolutely Nothing Anywhere Near Anything).
- Better wind conditions with higher and more predictable wind speeds and lower wind fluctuations due to the lower surface roughness of water.
- Economies of scale, i.e., the cost of a wind turbine is increasing slower than its power rating. Generally, larger wind turbines can more easily be transported and erected offshore than on land.

Normally, sites with shallow waters relatively close to the shore are preferred for offshore wind farms. An important factor is the transmission distance which strongly influences the grid connection costs. Still, there are incentives for siting wind farms further offshore. Environmental concerns such as visibility, noise disturbance, and impact on the marine flora and fauna are mitigated. In addition, near-shore areas are often subject to different established interests, involving military restrictions, recreational activities, maritime traffic, or coastal fishing. When technical challenges, such as the foundation of the wind turbines, will be overcome, future offshore wind farms may be built much further offshore, perhaps even on floating platforms at sea.

With more and larger remotely located wind farms, new solutions are needed to feed the generated power into the grid for onward transmission and distribution. Traditional high-voltage alternating current (HVAC) transmission (refer to Section 2.1) used in the first, smaller offshore wind farms is often reaching its limits. The main reason is the high reactive power demand of AC cables, which for long cables eventually would take up the entire current carrying capacity, such that no active power could be transmitted anymore. Therefore, voltage source converter (VSC) based HVDC transmission, commonly called VSC transmission (refer to Section 2.2.2), is the ideal means to transmit large amounts of electric power through long submarine cables. At the same time, VSC transmission systems assure a good power quality [6, 7], which is especially important with regard to the augmented penetration of wind power generation, which occassionaly can exceed 100 % of total

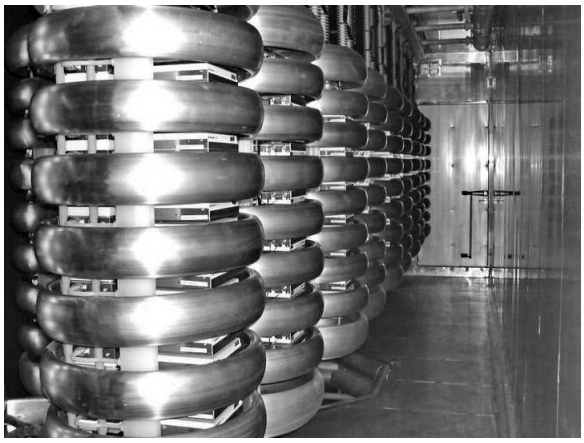

Figure 1.2: Inside a valve enclosure of a VSC station (courtesy of ABB).

electricity consumption in Denmark or northern Germany (peak penetration levels $>100\,\%$) [8]. Today, large wind farms are therefore required to contribute to the network stability and to handle grid faults in the same way as conventional power plants, which is one of the essential advantages of VSC transmission systems:

- Has full black-start capability, i.e., it can even start up against a dead network.
- The VSC substations at both ends of the HVDC transmission system can contribute to the regulation of the network frequency as they have the ability to control the active power flow. Short-term power demands can mainly be handled by rotational energy stored in the wind turbine rotors.
- By controlling the active power flow, HVDC connections can be operated very close to the physical limits of the cables. This increases the transmission capacity compared to HVAC connections, which need a certain margin for power flow fluctuations.
- VSC transmission systems can be connected to weak power grids. However, it may be beneficial from a system point of view to make the connection at a major substation further inland. This is no problem with DC cables, which are not affected by capacitive charging currents and can have any length required.
- Compared to new overhead transmission lines, it is much easier to obtain the necessary permits to build submarine or underground cables.
- The unsteady operating conditions in wind farms can cause variations in reactive power, which can deteriorate the power quality on the grid and cause flicker. The VSC substations can independently control the reactive power, which helps to stabilize the grid in its connection point by assisting in the voltage control of the AC network [9]. This is of special importance for the, generally, comparably weak grids along the coastlines.

HVDC transmission transfers power by converting AC to DC at one end and converting it back to AC at the other end. This power conversion is performed by solid state converter stations (see Fig. 1.2), which are costly and bulky. In addition, the high-frequency switching of the power semiconductor switches generates considerable losses [10]. In this thesis, a novel soft-switched VSC transmission system is investigated that differs significantly from conventional solutions as shown in

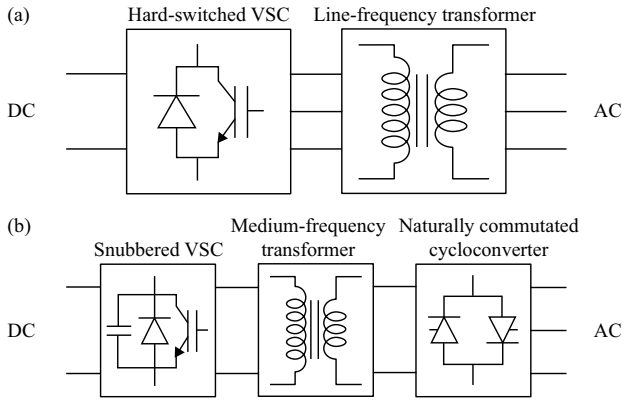

Figure 1.3: Overview of isolated AC/DC power conversion systems: (a) Conventional VSC system, (b) Mutually commutated converter system.

Fig. 1.3(a). The proposed mutually commutated converter (MCC) system shown in Fig. 1.3(b) aims to increase the system efficiency and at the same time reduce the initial costs as well as the footprint and weight of the converter platform, which is of particular importance for an offshore application. As a consequence, VSC transmission gets more competitive and attractive for the grid connection of large wind farms.

1.2 Objectives

The aim of this project is to apply an MCC system in a wind farm, providing a unique integrated solution for the generator drive systems, the turbine interconnection, and the power conversion for onward HVDC transmission. The objectives of this thesis focus mainly on finding technical solutions with regard to a specific application.

In principle, the feasibility of a compact MCC system as shown in Fig. 1.3(b) has already been confirmed prior to this thesis, both with simulations [11] and experimentally [12]. Nevertheless, several project objectives are directly concerned with MCC systems, thus making the results generally valid regardless of the specific application.

1. Practical implementation and evaluation of pulse width modulation (PWM) and space vector modulation (SVM) methods in a cycloconverter equipped with IGBTs (see [VI, IX, X] and Section 5.1).
2. Development of a modulation strategy that allows to replace the IGBTs in the cycloconverter with fast thyristors (see [V, VII], [13] and Section 4.5).

3. Modification, implementation, and evaluation of a prototype converter system operating with thyristors in the cycloconverter (see [VII], [14] and Section 5.2).

In case of an application in a wind farm, the MCC system will become distributed. A medium-frequency (MF) collection grid connects the converter station, equipped with a single-phase VSC and an MF transmission transformer, with the wind turbines, each containing a cycloconverter and an MF distribution transformer. The following project objectives are therefore focusing on issues regarding the application of a distributed MCC system in a wind farm.

4. Design and evaluation of an MF collection grid that has an acceptable level of transient overvoltages (see [IV], [15] and Section 3.2.1).
5. Magnetic, electric, and thermal design of MF transformers with suitable leakage inductances and parasitic capacitances (see [VIII] and Section 3.2.2).
6. Development of a strategy to commutate the VSC during low power generation (see [IV, V] and Section 3.2.3).
7. Design of a feasible wind farm layout (see Section 3.3).
8. Realisation of a study about the system efficiency and initial costs, showing that the proposed topology has considerably lower energy generation costs than conventional solutions for large winds farms distant to a strong grid connection point (see [II, III] and Section 3.2.5).

Summing up, the driving force of this work has been to further develop the MCC system and, based on it, establish a feasible and profitable solution combining the power collection and conversion in large wind farms.

1.3 Original contributions

The following list summarizes the key original contributions of this work. According to the author's knowledge, these have not been published prior to this thesis or the included publications.

1. System studies of distributed MCC systems in large wind farms:
   a) Investigations about the influence of different parameters on the electromagnetic oscillations in the MF collection grid as described in Section 3.2.1. Discussion about how these parameters can be modified and how this influences the system performance.
   b) Proposal of how to enable the VSC commutation during low power generation without auxiliary circuit, refer to Section 3.2.3.

   c) Proposal of a thyristor-controlled snubber capacitor, which controls the VSC commutation duration independent of the actual power generation, see Fig. 3.10. A thyristor-controlled snubber capacitor solves also the problem with the VSC commutation during low power generation, refer to Section 3.2.3.

   d) Loss calculations, both on the converter level [II] and system level [III].

   e) Calculation of converter ratings [II].

   f) Proposal of a wind farm layout as described in Section 3.3.

2. Implementation and experimental verification of an SVM method in an MCC system as described in [VI]. Interpretation of the measurement results.

3. Modulation of an MCC system with thyristors in the cycloconverter:

   a) Proposal of a current-clamping control strategy, as first described in [V], that solves the problem with the zero-crossings of the cycloconverter currents and respects that a thyristor must be reverse-biased for a certain duration before a positive voltage can be reapplied. Verification by simulations.

   b) Comparison of the current-clamping control strategy with other modulation methods regarding the maximum possible modulation ratio, see Table I in [VII].

   c) Construction of a prototype converter, including main circuit, cycloconverter gate drive, MF transformer and adaptation of control system, as described in Section 5.2 and in [VII].

   d) Identification of requirements for a successful implementation of the current-clamping control strategy, namely the need for precise measurement and prediction of the current vector [VII].

4. Investigation of quasi-discontinuous PWM (QDPWM) for MCC systems:

   a) Mathematical formulation of zero-sequence components for different clamping strategies in Table 4.1.

   b) Identification of vector sequence selection for different clamping strategies and comparison to SVM as shown in Fig. 4.6.

   c) Proposal of a load angle dependent choice of QDPWM strategy that corresponds with SVM, refer to Table 4.2.

5. Design of MF power transformers:

   a) Standardization of equations for analytical calculations of parasitic capacitances, see Tables III and IV in [VIII].

   b) Reformulation of the modified Steinmetz equation based on the form factor of the voltage waveform, according to Eq. (17) in [VIII].

1.4 Outline of the thesis

The contents of this thesis are organised as follows:

Chapter 2 gives a general overview of different transmission systems, particularly with regard to the suitability for the grid connection of large wind farms. The main focus is on VSC-based HVDC transmission systems.

Chapter 3 first describes the proposed MCC system for the grid connection of large wind farms and its principle of operation. Thereafter, technical and economical aspects are discussed in order to propose a suitable wind farm layout.

Chapter 4 gives an overview and comparison of different modulation methods for MCC systems. A modulation method considering all modulation constraints is proposed that does not require any turn-off capability in the cycloconverter valves.

Chapter 5 covers the experimental work carried out during this project.

Chapter 6 summarizes this thesis and provides some suggestions for future work.

1.5 Publications

This doctoral thesis has resulted in the following publications, presented in chronological order. Most of them have been published at international conferences. Those publications that are appended to this thesis for reference are provided with a link to the corresponding page number highlighted in grey. The format of the attached articles is rescaled from the original size to fit into the layout of this thesis.

[I] **S. Meier**, S. Norrga and H.-P. Nee, *"New Topology for more efficient AC/DC Converters for Future Offshore Wind Farms"* in *Proceedings of the 4th Nordic Workshop on Power and Industrial Electronics, Norpie '04*, Trondheim, Norway, June 2004.
→ appended to this thesis, see page 81.

[II] **S. Meier**, S. Norrga and H.-P. Nee, *"New Voltage Source Converter Topology for HVDC Grid Connection of Offshore Wind Farms"* in *Proceedings of the 11th International Power Electronics and Motion Control Conference, EPE-PEMC '04*, Riga, Latvia, September 2004.
→ appended to this thesis, see page 89.

[III] **S. Meier** and P. C. Kjær, *"Benchmark of Annual Energy Production for Different Wind Farm Topologies"* in *Proceedings of the 36th Annual Power Electronics Specialists Conference, PESC '05*, Recife, Brazil, June 2005.
→ appended to this thesis, see page 97.

[IV] **S. Meier**, *"Novel Voltage Source Converter based HVDC Transmission System for Offshore Wind Farms"*, Licentiate thesis, Royal Institute of Technology, Stockholm, Sweden, December 2005.

[V] **S. Meier**, S. Norrga and H.-P. Nee, *"Modulation Strategies for a Mutually Commutated Converter System in Wind Farms"* in *Proceedings of the 12th European Conference on Power Electronics and Applications, EPE '07*, Aalborg, Denmark, September 2007.
→ appended to this thesis, see page 107.

[VI] **S. Meier**, M. Kuschke and S. Norrga, *"Space Vector Modulation for Mutually Commutated Isolated Three-Phase Converter Systems"* in *Proceedings of the 39th Annual Power Electronics Specialists Conference, PESC '08*, Rhodes, Greece, June 2008.
→ appended to this thesis, see page 119.

[VII] **S. Meier**, S. Norrga and H.-P. Nee, *"Control Strategies for Mutually Commutated Converter Systems without Cycloconverter Turn-off Capability"* in *Proceedings of the 39th Annual Power Electronics Specialists Conference, PESC '08*, Rhodes, Greece, June 2008.
→ appended to this thesis, see page 127.

[VIII] **S. Meier**, T. Kjellqvist, S. Norrga and H.-P. Nee, *"Design Considerations for Medium-Frequency Power Transformers in Offshore Wind Farms"* in *Proceedings of the 13th International European Power Electronics Conference and Exhibition, EPE '09*, Barcelona, Spain, September 2009.
→ appended to this thesis, see page 135.

In addition, during the course of the work the author has co-authored the following publications:

[IX] S. Norrga, **S. Meier** and S. Östlund, *"A Three-phase Soft-switched Isolated AC/DC Converter without Auxiliary Circuit"* in *Proceedings of the 39th Annual Meeting of the Industry Applications Society, IAS '04*, Seattle, United States, October 2004.

[X] S. Norrga, **S. Meier** and S. Östlund, *"A Three-Phase Soft-Switched Isolated AC/DC Converter without Auxiliary Circuit"* in *IEEE Transactions on Industry Applications*, May/June 2008.

[XI] F. Meier, **S. Meier** and J. Soulard, *"Emetor - An educational web-based design tool for permanent-magnet synchronous machines"* in *Proceedings of the 18th International Conference on Electrical Machines, ICEM '08*, Vilamoura, Portugal, September 2008.

The author has also supervised or been involved in project works or master theses that resulted in the following reports:

- M. Kuschke, *"Practical implementation of a cycloconverter in a soft-switching isolated AC/DC converter"* [14].
- Z. Shuang, *"Mutually commutated converter equipped with thyristor-based cycloconverter"* [13].
- L. Nian, *"Transients in the collection grid of a novel wind farm topology"* [15].

2 Survey of transmission systems for wind farms

This chapter presents a survey of different transmission systems that are suitable for the grid connection of large wind farms. Both HVAC and HVDC transmission systems are covered, of which the latter are either line-commutated converter (LCC) or VSC based. Finally, different VSC topologies are investigated.

2.1 HVAC

Conventional HVAC transmission systems offer a simple and cost-efficient solution for the grid connection of wind farms. In principle, they consist of an AC wind farm collection grid, a transformer station and one or several three-core cross-linked polyethylene (XLPE) insulated HVAC cables, see Fig. 2.1. Unfortunately, the distributed capacitance of undersea cables is much higher than that of overhead power lines. This implies that the maximum feasible length and power transmission capacity is limited. The reactive power demand of HVAC cables increases both with the voltage level and the cable length. Thus, for increasing transmission distances and voltage levels, reactive power compensation is required at both cable ends [III]. The reactive power compensation can be realized by a static VAr compensator (SVC) for example, both offshore and onshore if necessary.

HVAC transmission has so long been the self-evident choice for offshore wind farms, since it is the most favorable and competitive solution for the grid connection of

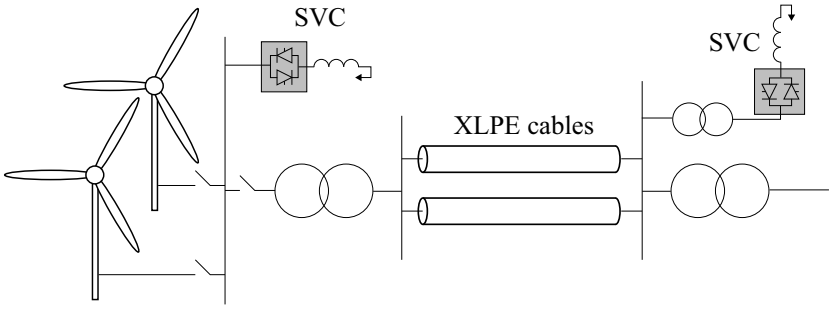

Figure 2.1: Priciple of an HVAC transmission solutions.

smaller wind farms located close to shore. Today, this comprises distances of up to 100 km and power transmission capacities of up to 200 MW [8]. For larger and more remote wind farms, transmission losses are increasing quickly and new solutions for the grid connection become necessary.

2.2 HVDC

Looking at HVDC transmission systems, there a two different technical solutions which are either based on current source converters (LCC) or voltage source converters (VSC).

2.2.1 LCC-based HVDC

Classical HVDC transmission technology is based on naturally commutated thyristors. The name line-commutated converter originates from the fact that the thyristors need an alternating voltage source in order to commutate. Therefore, LCC-based HVDC can only transfer power between two active AC networks. This is less useful for a wind farm since the offshore AC grid needs to be powered up prior to a possible startup. A further disadvantage of LCC-based HVDC is that it cannot provide independent control of active and reactive power. In addition, it produces extensive amounts of harmonics which have to be filtered, thus making the converter stations relatively large.

In order to find a feasible approach for an LCC-based HVDC grid connection of wind farms, different solutions have been proposed, e.g. a combination with a static compensator (STATCOM), see Fig. 2.2(a). The STATCOM provides both the necessary commutation voltage to the LCC and the reactive power compensation to the offshore grid. It can also provide limited active power support to the offshore grid during transient conditions [16]. As shown in Fig. 2.2(a), the cable transmission is often monopolar with only one metallic conductor between the converter stations, using the ground as the return path for the current.

For connecting large wind farms over long distances, LCC-based HVDC with shunt capacitors, STATCOM support or other reactive equipment combines the technical advantages of classical HVDC with those of an equivalent VSC-based transmission system. Since classical HVDC transmission is a well established technology, it offers high reliability and requires little maintenance. Compared to VSC transmission systems, LCC-based HVDC transmission has much lower power losses (i.e., about 0.6 - 0.7 % of the rated HVDC transmission capacity (per station) at rated load [17]) and for high ratings it has comparably low capital costs. However, based on the overall system economics, LCC-based HVDC transmission becomes only interesting for power capacities above approximately 600 MW [8].

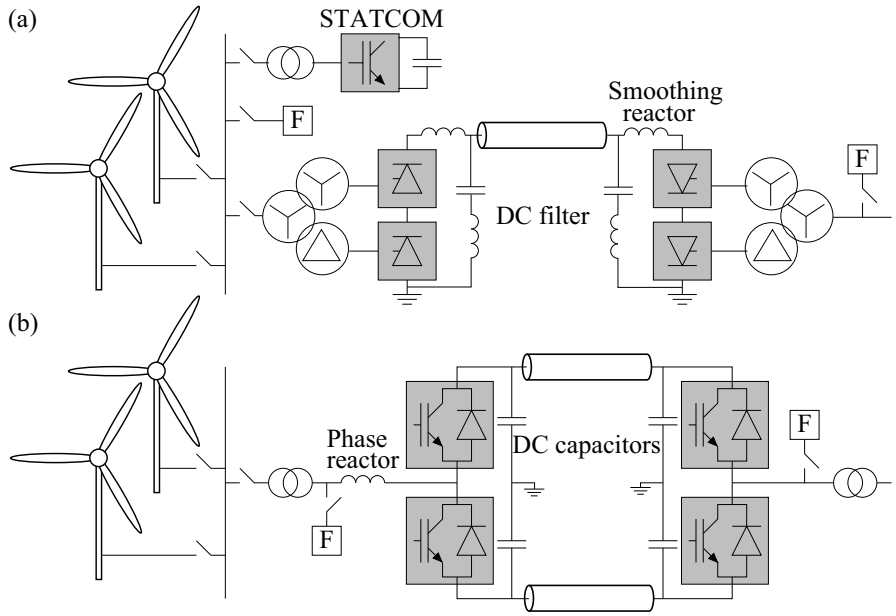

Figure 2.2: Principles of HVDC transmission systems: (a) Classical LCC-based system with STATCOM, (b) VSC-based system. (F = Filter)

LCC-based HVDC transmission has been installed frequently, primarily for bulk power transmission over long geographical distances and for interconnecting non-synchronised or isolated power systems. So far, there is no experience regarding LCC-based HVDC transmission in combination with wind power.

2.2.2 VSC-based HVDC

As discussed in Section 1.1, VSC-based HVDC transmission offers many advantages and is gaining more and more attention, not least in context with the grid connection of large wind farms. This comparatively new technology (first commercial installation in 1999 [18]) has only become possible by the development of the IGBT, which can switch off current. This means that there is no need for an active commutation voltage. Today, VSC-based HVDC is marketed by ABB under the name "HVDC Light" and by Siemens under the name "HVDC Plus". Fig. 2.2(b) shows the principle of a VSC-based HVDC transmission system.

Compared to conventional HVDC, IGBTs allow much higher switching frequencies, which reduces the harmonic distortion and consequently the filter requirements on the AC side. However, the high-frequency PWM switching results in comparably high converter losses, which are in the range of approximately 1.6 % of the rated

HVDC transmission capacity (per station) at rated load [17]. The total efficiency of VSC-based HVDC is therefore less than that of an LCC-based system. Furthermore, the cost of a VSC is relatively high due to the more advanced semiconductor valves required. In order to handle the high voltage, multiple IGBTs have to be connected in series, which makes the valves expensive, since complex gate drives and voltage sharing circuitries are required.

Looking at the overall system economics, VSC-based HVDC transmission systems are most competitive at transmission distances over 100 km and power levels of between approximately 200 and 900 MW [8]. However, the application of VSC-based systems may already be advantageous for shorter transmission distances depending on the specific project conditions. To date, no pure VSC-based HVDC transmission system is in operation in conjunction with the grid connection of a wind farm. However, several projects are in the planning stage right now and a demonstration installation has been put into operation back in the year 2000 [6, 7].

2.2.3 Basic VSC topologies

The application of the IGBT, which is a self-commutated semiconductor device, makes many different topologies suitable for VSC. Different solutions, such as two-level, three-level, and multi-level converters, have extensively been discussed and compared in terms of harmonic spectrum, DC capacitor volume, commutation inductance, costs, and footprint, see e.g. [19]. Regarding multi-level solutions, four main topologies are known [20]: Diode-clamped, capacitor-clamped, cascaded H-bridge, and modular multilevel converter (M^2LC [21]). With such an abundance of different technical solutions, it is a good idea not to depart from the core topologies of the main manufacturers, if one hopes to have his ideas ultimately implemented [22].

According to Ooi [22], manufacturers will keep developing their core topologies of VSC:

- *The two-level three-phase bridge of Fig. 2.3:* This simple topology has been widely used in many applications, e.g. in the ABB product "HVDC Light" [17]. The phase outlets can either be connected to the positive or negative DC-link terminal, thus generating a two-level output voltage ($+U_d/2$, $-U_d/2$), which can be modulated by a PWM or SVM scheme.
- *The three-level three-phase bridge of Fig. 2.4:* By clamping the neutral point of the DC-link terminal with diodes, it is possible to generate a three-level output voltage ($+U_d/2$, 0, $-U_d/2$), which can be modulated by a PWM or SVM scheme.
- *The cascaded single-phase H-bridge of Fig. 2.5(a):* Extending a diode- or capacitor-clamped VSC to more levels drastically increases the complexity and the number of clamping diodes or flying capacitors. Therefore, a strictly modular construction is important in order to enable scaling to different power and voltage levels, using the same hardware [20]. A common solution is the

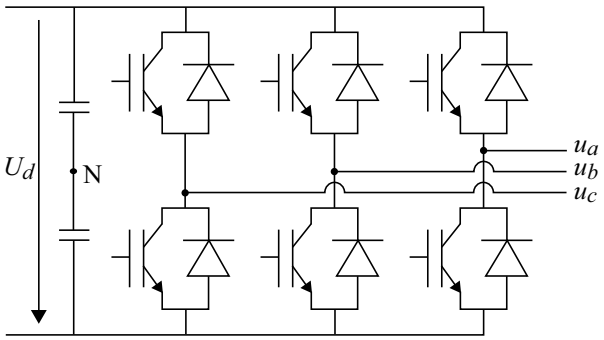

Figure 2.3: Classical two-level three-phase VSC.

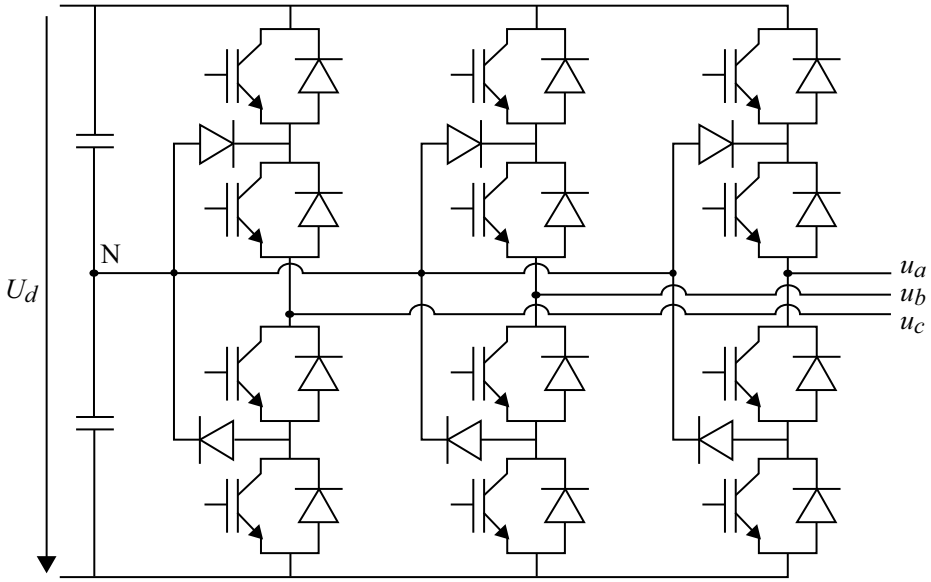

Figure 2.4: Neutral point clamped three-level three-phase VSC.

cascaded H-bridge shown in Fig. 2.5(a), which is fully modular (one module is highlighted in grey). However, every H-bridge module needs its own isolated DC power supply. Recently, a novel multilevel VSC topology called M^{2}LC [20, 21] has been proposed, which has a common DC-link, but no DC-link capacitors, see Fig. 2.5(b). The DC-link voltage is directly controlled via the switching states of the submodules [20], which therefore do not need an isolated DC power supply. The M^{2}LC topology is utilized in the Siemens product "HVDC Plus" [23].

The example of the M^{2}LC topology shows that there is no problem to get good ideas commercialized, if only they are based on a core topology of a manufacturer and offer significant improvements. This applies also to the two-stage isolated mutually commutated VSC shown in Fig. 2.6, which was first proposed in its current state by Norrga [24]. It is a further development of the classical two-level three-phase VSC

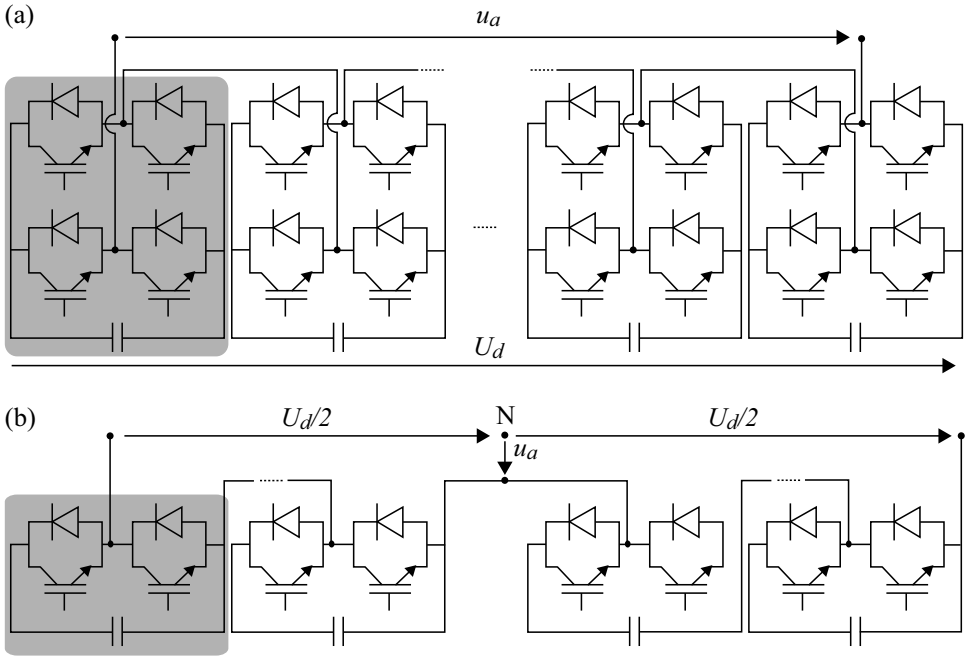

Figure 2.5: Single-phase multilevel VSC: (a) Cascaded H-bridge, (b) M^2LC.

shown in Fig. 2.3.

The basic principle of operation is that a single-phase VSC generates an MF square-wave voltage ($+U_d/2$, $-U_d/2$), which energizes the MF transformer. The VSC valves are equipped with parallel snubber capacitors, which allow the semiconductor switches to be turned off under zero-voltage conditions. The MF transformer is then connected to a three-phase cycloconverter, which can be commutated in order to obtain the desired three-phase alternating voltage. The cycloconverter valves do not need any turn-off capability and can be entirely naturally commutated, which makes it suitable to utilize anti-parallel fast thyristors.

Even though a two-stage conversion system normally has more components and tends to have higher losses than a single-stage conversion system, the MCC system in Fig. 2.6 has several advantages compared to a classical two-level VSC:

- Considerably reduced switching losses due to a soft-switching commutation scheme (refer to [II]), allowing snubbered zero-voltage switchings of the VSC valves and natural commutations of the cycloconverter valves.
- Cheaper, lighter, and more compact single-phase MF transformers compared to three-phase line-frequency transformers (refert to [VIII]).
- Reduction of series-connected IGBT valves (refer to [II]), which are expensive and require complex gate drives and voltage sharing circuitries.
- The thyristors in the cyclcoconverter are comparably cheap, have low conduction losses, and their robustness and reliability is unsurpassed.

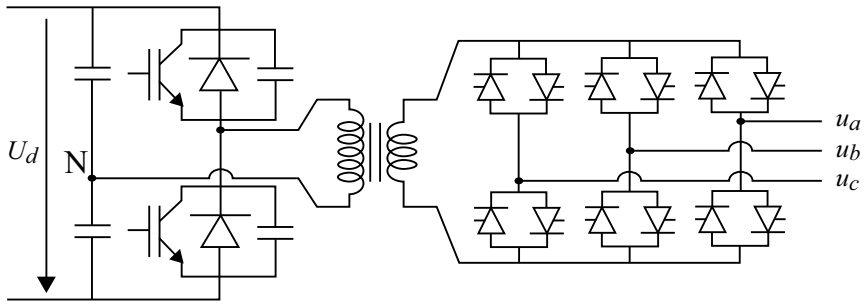

Figure 2.6: Two-level three-phase isolated mutually commutated VSC.

2.3 Conclusions

This chapter intends to present a short survey of different transmission systems for large wind farms, which is an area of growing worldwide interest. Table 2.1 lists some interesting references for further reading, especially with regard to relevant projects. Today, there are still not many large *offshore* wind farms in operation, and the few installations are exclusively using HVAC transmission. However, since the responsibility for network connection of offshore wind farms nowadays often lies with the transmission system operators (TSO), the network connection can be optimized irrespective of the particular wind farms involved [4]. Hence, TSO's will rather provide "seaborne power sockets", to which complete wind farms can be connected [4]. In this case, HVDC transmission is the ideal solution. Further in the future, these power sockets could be linked together in order to create an offshore HVDC supergrid [8], ranging from Scandinavia in the north of Europe down to northern Africa. Such an offshore supergrid based on LCC or VSC (or a combination of the two) HVDC transmission systems, could connect offshore wind farms as well as large-scale photovoltaics in northern Africa.

VSC-based HVDC transmission is the most recent technology and has large potential for further development. Therefore, the basic VSC topologies have been introduced in Section 2.2.3 in order to guide the reader towards the topology that is proposed for the grid connection of large wind farms in the next chapter.

Table 2.1: Further reading about transmission systems, especially for offshore wind farms.

[8] (p. 479 ff)	General textbook description.
HVAC	
[25]	Comparison with HVDC transmission.
[26]	Project: 160 MW Horns Rev wind farm.
LCC-based HVDC	
[10, 16]	Feasibility investigations.
VSC-based HVDC	
[6, 7]	Application of HVDC Light in offshore wind farms.
[18, 27, 28]	Project: 20 MW Gotland HVDC Light. First commercial small-scale DC transmission.
[29, 30]	Project: 7.2 MW Tjæreborg HVDC Light. Demonstration installation for wind farm connection.
[4]	Project: 400 MW Borkum offshore "power socket". Links up the world's largest offshore wind-farm area.

3 System properties

A distributed version of a mutually commutated soft-switching converter system seems to be tailored to the particular needs for the power collection and HVDC conversion in large wind farms. At first, the operation principle of this topology is described, such as the mutual commutation of the VSC and the cycloconverters. Some basic voltage and current waveforms from measurements further illustrate the operation principle. Then, different system aspects which are specific to the application in a wind farm are investigated, such as the design of the collection grid, the MF transformers, and the VSC commutation at low load. Finally, a technically feasible wind farm layout is proposed, considering economical aspects such as initial costs and conversion losses.

A simplified schematic of the proposed topology for the power collection and HVDC grid connection of large wind farms is shown in Figure 3.1. This topology represents a distributed version of the two-level three-phase isolated MCC system shown in Fig. 2.6. The application in a wind farm as an integrated solution for the drive systems of the wind turbine generators, the electric turbine interconnection, and the conversion stage for onward HVDC transmission was first considered by Norrga [24] and is described in detail in [I,IV].

As shown in Fig. 3.1, the drive train of the wind turbine is housed in its nacelle. It comprises a gearbox, a generator (of arbitrary type, but preferably a squirrel-cage induction generator), and a cycloconverter, which allows every wind turbine to operate with variable voltage and variable frequency. A filter connected between the cycloconverter and the generator could limit the harmonic distortion in the cycloconverter output voltage and reduce undesired losses in the generator. The connection between the wind turbines and the collection grid can be integrated in the bottom of the wind turbine towers. There, an MF distribution transformer increases the voltage to 33 kV and a circuit breaker enables the wind turbines to disconnect from the collection grid, e.g. during faults, at low wind speeds, or for maintenance.

The collection grid has a radial structure with several wind turbines building up a chain, refer to Fig. 3.14. The single-phase MF collection grid connects all wind turbines to a central converter station, which comprises the main circuit breaker, an MF transmission transformer, and a single-phase VSC, see Fig. 3.1. The main circuit breaker allows the wind farm to be shut down, e.g. during serious faults or

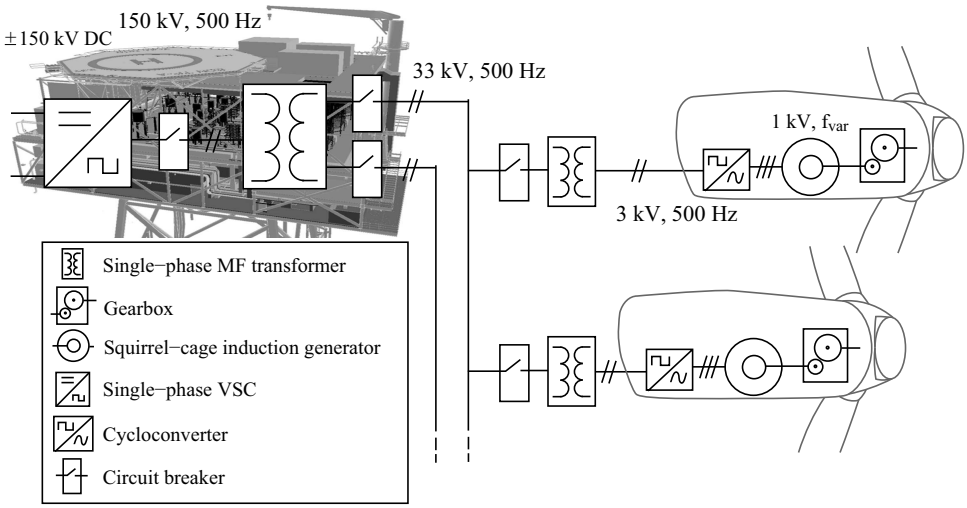

Figure 3.1: Simplified schematic of the proposed topology for the power collection and HVDC conversion in large wind farms.

on demand of the TSO. The MF transmission transformer raises the voltage of the collection grid to 150 kV, which is half the DC link voltage. The high-voltage side of the transformer is connected to a single-phase VSC, whereas one of the transformer terminals is connected to the midpoint in the DC link created by bus-splitting capacitors (see Fig. 2.6). These capacitors provide the necessary direct voltage source for the dynamics of the system and govern the voltage ripple on the HVDC link.

3.1 Principle of operation

In the proposed topology in Fig. 3.1, the VSC converts the direct voltage to an MF alternating voltage that magnetizes the MF collection grid. The MF transmission and distribution transformers provide isolation and voltage transformation. Finally, the MF alternating voltage is converted to desired three-phase voltages by the cycloconverters.

By consistently commutating the VSC and the cycloconverters in alternation, see Fig. 3.2, it is possible to mutually set up the conditions for soft commutations for all semiconductor devices [11]. Soft commutation means to turn on or turn off the semiconductor devices with minimized switching stress, i.e., at zero-voltage or zero-current conditions [31]. Thereby, the switching losses are considerably reduced. In the proposed topology, the cycloconverters can be entirely operated by natural commutations, whereas snubbered or zero-voltage commutations are always enabled for the VSC. The special case of a VSC commutation during low energy generation

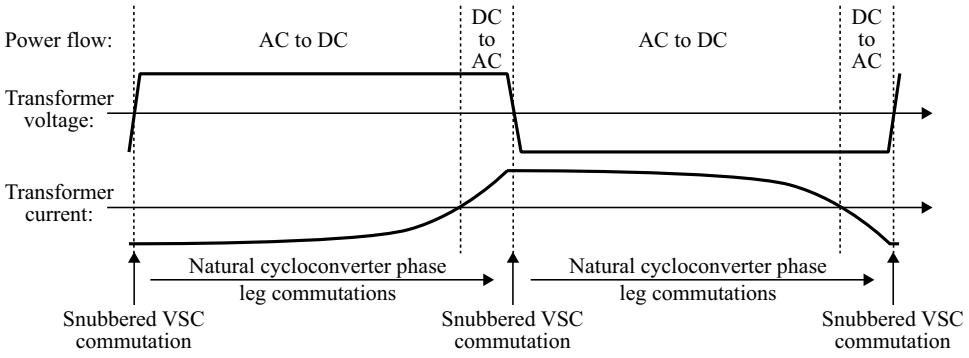

Figure 3.2: Soft-switching commutation cycle.

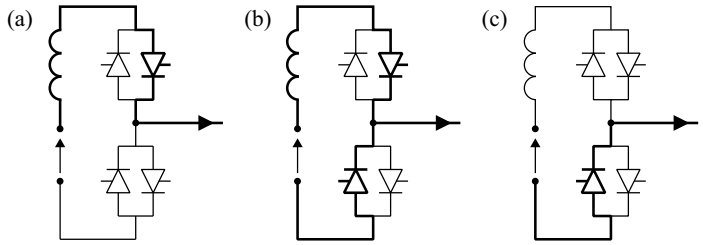

Figure 3.3: Sequence of a cycloconverter phase leg commutation.

is discussed in Section 3.2.3. Different suitable modulation strategies for MCC systems are described in Chapter 4.

3.1.1 Cycloconverter phase leg commutation

The sequence of an arbitrary cycloconverter phase leg commutation is shown in Fig. 3.3. For simplicity, the leakage inductances of the transformers and the distributed cable inductance of the collection grid are represented as an equivalent inductance, which determines the current slope during the cycloconverter phase leg commutations. At the same time, the output voltage of the VSC is represented as a constant voltage during the entire commutation duration.

In order to be able to naturally commutate a cycloconverter phase leg, the sign of the transformer voltage has to be opposite to the sign of the respective line current, as it is the case in Fig. 3.3(a). The cycloconverter phase leg commutation is initiated by turning on the non-conducting valve in the direction of the current through the phase terminal. The transformer voltage will then appear across the equivalent inductance and make the incoming valve gradually take over the current, refer to Fig. 3.3(b). Finally, the initially conducting valve turns off as the current through it goes to zero, see Fig. 3.3(c).

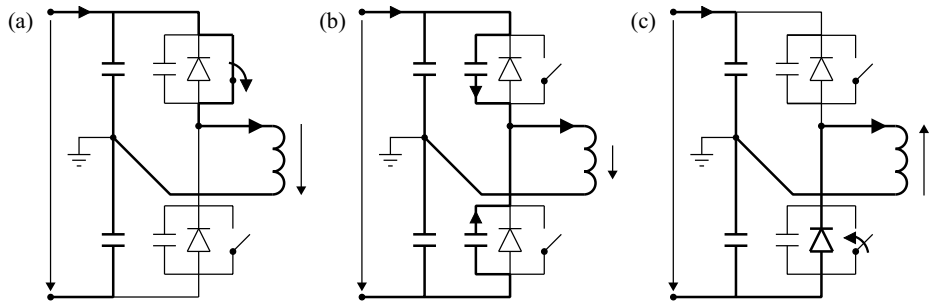

Figure 3.4: Sequence of a VSC commutation.

Successive commutations of the cycloconverter phase legs eventually lead to a reversal of the transformer current, see Fig. 3.2. Now the transmission transformer voltage and current have the same sign, which means that the instantaneous power flow is directed from the DC to the AC side.

3.1.2 VSC commutation

The conditions for a snubbered commutation of the VSC are fulfilled whenever the transmission transformer voltage and current have the same sign. This is the case in Fig. 3.4(a), where both the transmission transformer voltage and current are positive. The VSC commutation sequence is started by turning off the conducting valve under zero-voltage conditions. The transformer current is thereby diverted to the snubber capacitors as shown in Fig. 3.4(b), which are getting charged or discharged, respectively. When the transformer voltage has fully swung to the opposite, the snubber capacitors in the incoming valve will be completely discharged and the diodes can take over the current, refer to Fig. 3.4(c). Now, the instantaneous power flow is directed from the AC to the DC side, see Fig. 3.2. Finally, the IGBTs that are anti-parallel to the conducting diodes can be gated on at zero-voltage and zero-current conditions, thus preparing the VSC for a subsequent current reversal due to the cyloconverter phase leg commutations. The reversal of the transformer voltage after the VSC commutation establishes the possibility for natural commutations of the cycloconverter phase legs. Thus, the commutation cycle can be repeated.

The VSC commutation is governed by the snubber capacitance and the transmission transformer current. Unfortunately, the commutation of the VSC may become unduly lengthy with a small transformer current, since the recharging of the snubber capacitors becomes slower, refer to Section 3.2.3.

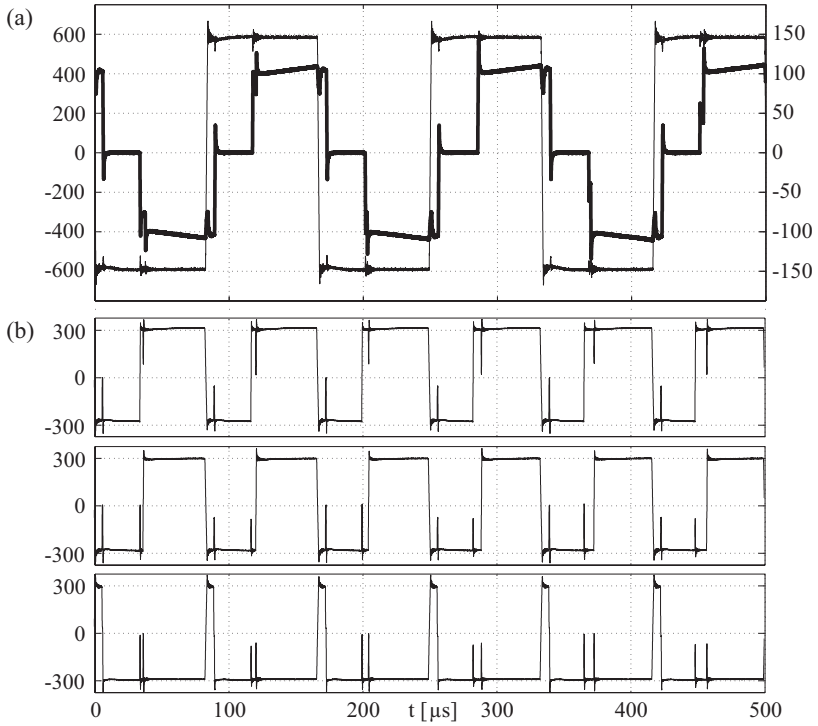

Figure 3.5: Measured waveforms: (a) Transformer voltage [V] (left scale) and transformer current [A] (bold, right scale), (b) Cycloconverter phase voltages [V].

3.1.3 Basic waveforms

In order to further illustrate the operation principle of the proposed topology, some basic waveforms from measurements on a prototype converter system (*Prototype I*, refer to Section 5.1) are shown in Fig. 3.5. The transformer voltage is basically a square wave with a period of 167 μs, corresponding to an operating frequency of 6 kHz. As expected, the transformer voltage and current have the same sign before a VSC commutation. The overall power flow is directed from the DC to the AC side, which corresponds with the experimental setup.

In Fig. 3.5(b), the three cycloconverter output voltages are shown, which have half the voltage amplitude of the transformer voltage. It can be noticed that one of the edges of each voltage pulse during a commutation period is due to the VSC commutation, while the other edge is due to the cycloconverter commutation. Further waveforms can be found in [II,IV,V] from simulations and in [VI,VII] from measurements.

3.2 System aspects

In this section, different aspects regarding the application of the proposed MCC system in a wind farm are investigated. It is discussed to what extent the advantages of MCC systems presented in Section 2.2.3 outbalance the complications from distributing the converter system over an entire wind farm. The following system aspects of a distributed MCC system are investigated:

Medium-frequency collection grid: The effect of switched voltages applied to cables is well known since the early unexpected insulation failures of inverter-fed AC motor drives with long motor leads. Voltage harmonics from switched voltages interfere with cable resonances, which results in transient overvoltages, refer to Section 3.2.1.

Medium-frequency transformer: Single-phase MF transformers are not only cheaper than three-phase transformers operating at line frequency (refer to Section 3.2.5), they are also more compact and have a lower weight, which is especially advantageous in offshore environments. However, the insulation of MF transformers is exposed to steep voltage slopes and transient overvoltages, which requires a careful winding design as discussed in Section 3.2.2.

Switching losses: Although an MCC system is a two-stage conversion system, the switching losses can be considerably reduced by a soft-switching commutation scheme, refer to Section 3.2.4. The VSC switching losses during low power generation may be somewhat increased depending on the commutation strategy, refer to Section 3.2.3.

Cycloconverters: In the cycloconverters, fast thyristors are preferred to other switching devices since they are comparably cheap, robust, reliable, and have low conduction losses at high current levels, refer to Section 3.2.4. With a special modulation method, the thyristor-based cycloconverters can be satisfactorily commutated despite their absence of turn-off capability, refer to Section 4.5.

Voltage source converter: The series-connected IGBT valves in the VSC are expensive and require complex gate drives and voltage sharing circuitries. Therefore, a VSC with a single phase leg is highly desirable, refer to Section 3.2.5.

3.2.1 Medium-frequency collection grid

One of the objectives of this work has been to design a single-phase MF collection grid that has an acceptable level of transient overvoltages. A comparison with measurements on a buried sea cable shows that the cable models included in the power system simulation software *PSCAD* [32] are sufficiently accurate for transient studies. Based on simulations of the MF collection grid, a solution is proposed

that limits the transient overvoltages in all operating points to an acceptable level. Accordingly, a suitable wind farm layout is proposed in Section 3.3.

Background

Transients occuring in the collection grids of large wind farms have been recently investigated [33,34], considering both fault conditions as well as switching operations during normal operation, such as energizing feeders. Contrary to these comparably infrequent events, the cables in a distributed MCC system are continuously exposed to a switched voltage from a VSC. The effects of switched voltages applied to cables are well known from inverter-fed AC motor drives with long motor leads, see e.g. [35].

The steep slopes of a switched voltage inherently cause voltage harmonics, which interfere with resonances between the cable capacitance and inductance of the MF collection grid, resulting in transient overvoltages [IV]. Fig. 3.6 shows results from a frequency domain analysis of an MF collection grid with a single feeder, where 10 wind turbines are equally distributed along an 11 km long cable [IV]. Assuming a fast VSC commutation, the harmonic spectrum of the MF alternating voltage will be close to the one of a square-wave voltage, which consists of odd harmonics with amplitudes that are decreasing inversely proportional to their harmonic order, see Fig. 3.6. In addition, the same figure shows different voltage transfer functions of the collection grid. A voltage transfer function is the ratio between a wind turbine voltage and the output voltage of the VSC as a function of the frequency. For a cable configuration as in Fig. 3.6, the fifth harmonic is amplified from 0.2 p.u. to over 3.6 p.u., which causes high transient overvoltages. Also the third, seventh, and fifteenth harmonics are increased with more than 10 % of the fundamental voltage.

The occurrence of transient overvoltages in the MF collection grid has been previously investigated in a comprehensive way [IV], arriving at the following conclusions:

- The resonance frequencies change depending on the actual configuration of the collection grid. Therefore, only certain predefined grid configurations should be allowed, preferably with cable feeders of the same length. It should be avoided to disconnect parts of a feeder, since this changes the voltage transfer functions of the collection grid.
- At higher frequencies, the resonances are more and more damped due to the frequency dependence of the cable parameters, see Fig. 3.6. Therefore, it is important to design a collection grid with few and small resonances, which preferably appear at high frequencies.
- The longer the cables, the lower the frequencies of the resonances. This is a limiting factor for how long a cable feeder can be in an MF collection grid.

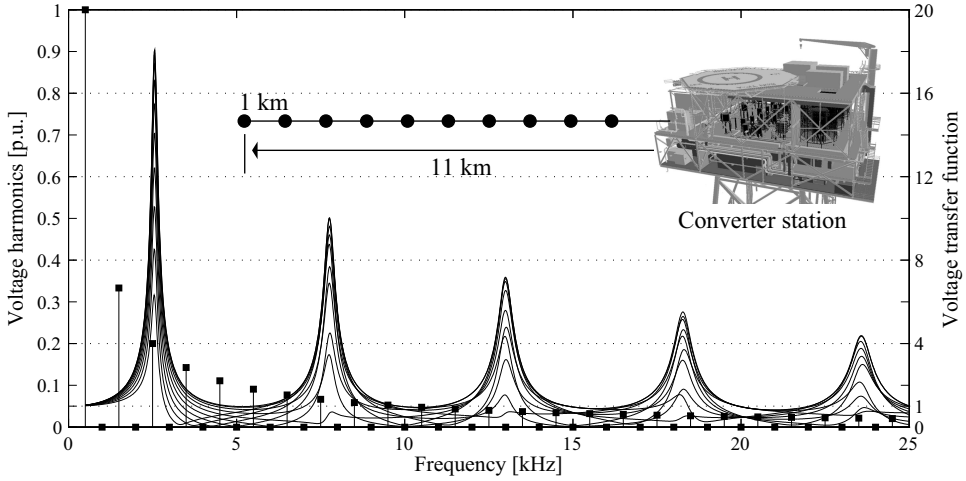

Figure 3.6: Interference between harmonic spectrum and voltage transfer functions in an MF collection grid [IV].

However, a shorter cable does not always signify lower transient overvoltages compared to a longer cable, cf. Fig. 3.9.

- The rise time of the MF alternating voltage depends on the snubber capacitance and the transformer current (i.e., the actual power generation). It is an important factor for influencing the harmonic spectrum of the collection grid voltage.
- In order to reduce transient overvoltages, the rise time of the collection grid voltage should be at least three times the time it takes a voltage pulse to travel the length of the cable [36]. This is not technically feasible in a wind farm collection grid with cable lengths up to 10 km or more, since the VSC commutation would take too long time.

Verification of the PSCAD cable model with measurements

The power system simulation software PSCAD contains three different types of distributed transmission line models, with the frequency-dependent (phase) model being the most advanced and accurate time domain model [32]. This model is based on a detailed description of the real cable parameters, such as geometrical layout and material properties, see Fig. 3.7.

In order to verify the suitability of the PSCAD cable model for transient analysis, results from simulations have been compared with measurement on a 162 m long buried three-phase sea cable from ABB. The XLPE-insulated cable is rated at 24 kV and has 240 mm^2 solid aluminum conductors and 85 mm^2 copper screens [37]. It is buried in a depth of between 0.3 to 0.5 m in relatively dry soil with an assumed ground resistivity of 200 Ωm, see Fig. 3.7. According to Fig. 3.8, the simulations

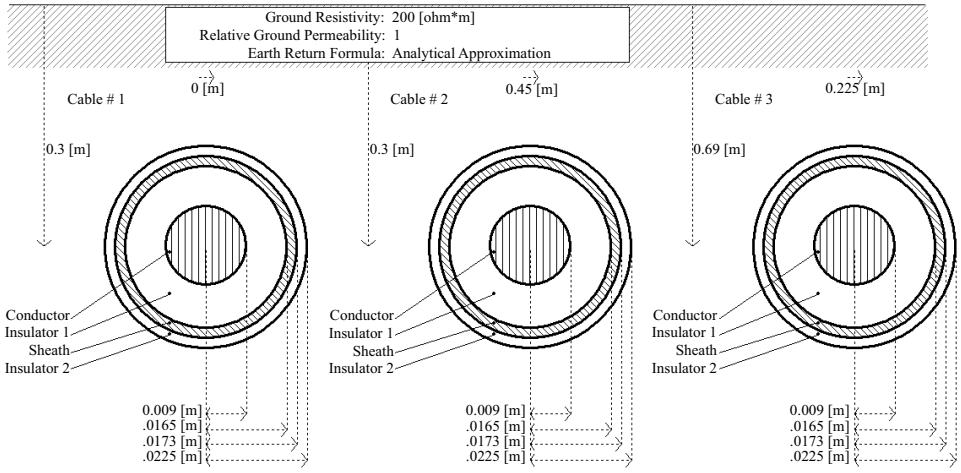

Figure 3.7: Graphical definition of a cable system in the PSCAD cable configuration editor [32]. Here, the three-phase submarine cable configuration on which the measurements in Fig. 3.8 were performed is shown.

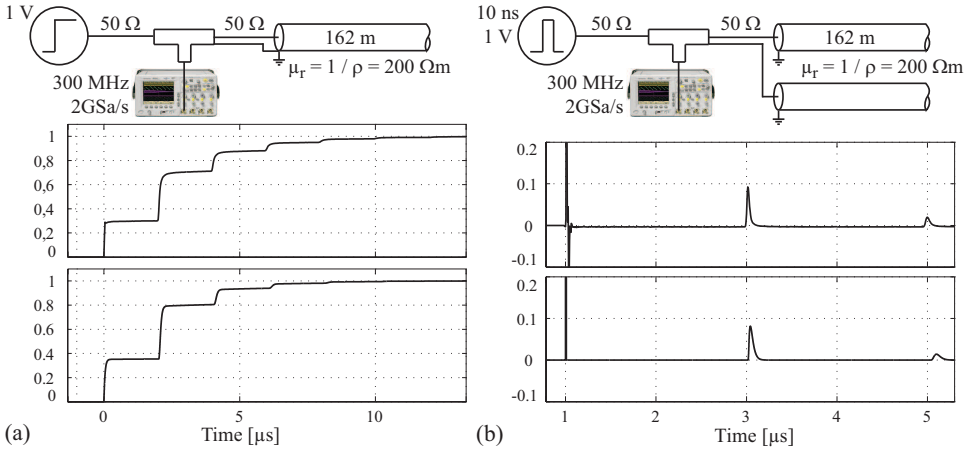

Figure 3.8: Setup for (a) step response and (b) pulse response measurements on a 162 m long buried three-phase sea cable (top). Comparison between measurements (middle) and simulations (bottom).

and measurements show good agreement both regarding the step response and the pulse response, which makes the frequency-dependent (phase) model in PSCAD suitable for transient analyses.

Simulations in PSCAD

For an MF collection grid with a rated voltage of 33 kV, single-core XLPE-insulated submarine cables from ABB [37] have been chosen and implemented in PSCAD for

Table 3.1: Choice of single-core submarine cables with copper conductor and a nominal voltage of 30 kV ($U_m = 36$ kV) [37].

Conductor cross-sectional area [mm^2]	Current rating [A]	Number of connected wind turbines
95	508	1-4
120	577	5
185	734	6
240	853	7
300	972	8
400	1116	9-10

simulations. The cross-sectional area of the copper conductor has been chosen depending on the number of wind turbines that are connected to the cable, refer to Table 3.1. The further out on a cable feeder, the smaller the cross-sectional area of the conductor. The smallest cable with a cross-sectional area of 95 mm^2 can carry the nominal current from up to four wind turbines. Table 3.1 shows the current rating for single-core cables with wide spacing, non-magnetic armour, and an armour resistance corresponding to 50 % of the conductor resistance. It was assumed that the cable laying depth is 0.5 m, the ground temperature 20 °C, and the ground thermal resistivity 0.7 Km/W. Such realistic conditions allow an increase of the current rating by approximately 25 % compared to the continuous current ratings calculated according to IEC 60287 under standard conditions (20 °C ground temperature, 1 m laying depth, and 1 Km/W thermal resistivity). The ground resistivity of the seabed soil is assumed to be 0.2 Ωm. In practice, the resistivity varies widely and is determined by the content of electrolytes (moisture, minerals and dissolved salts) in the seabed soil. For further details about different rating factors, the geometrical layout, and the electrical parameters of the chosen cables, refer to [37].

Fig. 3.9 shows results from simulations of transient overvoltages in the MF collection grid, depending on the cable length and the voltage slope during the VSC commutation. The simulations were performed at no-load conditions, i.e., no wind turbines were connected to the MF collection grid. The length of the cable feeder varies between 5 to 10 km. Assuming that the wind turbines are located at intervals of 1 km, it would be possible to connect between 5 to 10 wind turbines to one cable feeder. The voltage slope during the VSC commutation was varied between 0.4 and 0.2 kV/μs. With a frequency of 500 Hz and a voltage level of 33 kV of the MF collection grid, the VSC commutation would consequently occupy between 16.5 % and 33 % of the commutation interval.

Fig. 3.9 shows that the resonances in the MF collection grid, as expected, strongly depend on the cable length. For the same cable length, on the other hand, the transient overvoltages can also vary considerably depending on the voltage slope of

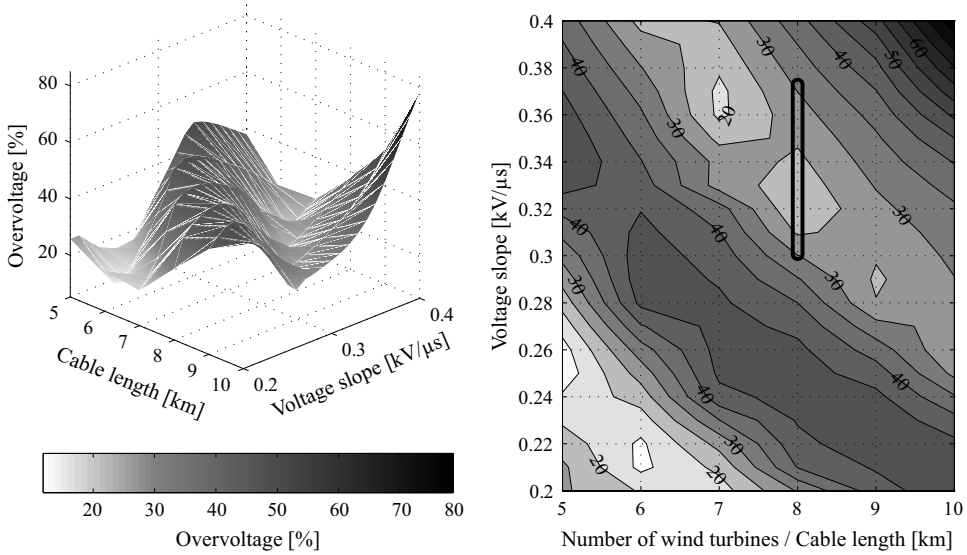

Figure 3.9: Amount of transient overvoltages in the MF collection grid as a function of the cable length and voltage slope during the VSC commutation.

the MF alternating voltage. Therefore, it is inevitable to control the voltage slope during the VSC commutation independent of the actual power generation, in order to be able to limit the transient overvoltages (light gray areas in Fig. 3.9).

Voltage slope control of the MF alternating voltage

A possibility of controlling the voltage slope during the VSC commutation independent of the actual power generation is shown in Fig. 3.10. A thyristor-controlled snubber capacitor, which is an original contribution, allows to control the duration of the VSC commutation and, consequently, the slope of the MF alternating voltage. Assuming that the cable feeders have a length of 8 km, a voltage slope between 0.375 and 0.3 kV/μs would limit the transient overvoltages to below approximately 30 %, refer to Fig. 3.9. For a wind farm that should be able to operate down to 10 % of the rated transformer current, two different configurations of snubber capacitors are proposed according to Fig. 3.10(a). Both snubber configurations have a total capacitance of 100 %, i.e., the value that limits the voltage slope to the upper limit during operation with nominal transformer current.

A thyristor-controlled snubber capacitor consists of thyristors in order to connect parallel capacitors, and anti-parallel diodes that allow the snubber capacitors to be discharged during the turn-on of the VSC valve. Both the thyristors and the diodes have to support the full DC-link voltage, but their current rating can be comparably small since they only conduct current during every second commuta-

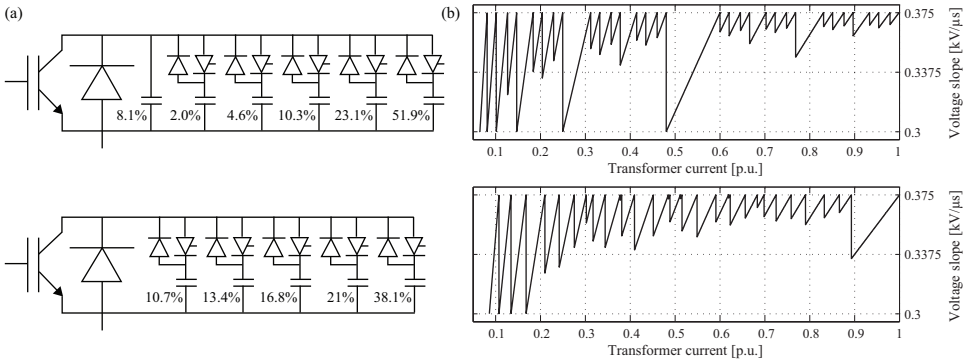

Figure 3.10: Voltage slope control during the VSC commutation: (a) Thyristor-controlled snubber capacitor with (top) or without (bottom) fixed capacitor, (b) Voltage slope as a function of the transformer current.

tion period, i.e., when they charge or discharge the snubber capacitors during the VSC commutation. In addition, the transformer current splits in half (charging, respectively discharging the snubber capacitors) and is proportional to the rating of the snubber capacitor in the respective leg (i.e., if the snubber capacitor is rated at 2 %, the current through the corresponding thyristor and diode will not exceed 2 % of the maximum snubber current).

The snubber configuration on top of Fig. 3.10(a) consists of five thyristor-controlled snubber capacitors and a fixed snubber capacitor. Such a configuration is more beneficial with regard to leakage inductances than the snubber configuration on the bottom of Fig. 3.10(a), which only consists of five thyristor-controlled snubber capacitors. Both snubber configurations can keep the voltage slope within the desired limits up to nominal transformer current, see Fig. 3.10(b). In order to ensure fast VSC commutations, the voltage slope was kept as close as possible to the upper limit of the reference band ($0.375\,\mathrm{kV}/\mu\mathrm{s}$). In addition, thyristor-controlled snubber capacitors inherently solve the problem with the VSC commutation during low power generation, refer to Section 3.2.3.

3.2.2 Medium-frequency transformers

One of the objectives of this work has been to investigate the magnetic, electric, and thermal design of MF transformers. Since the transformers in the MCC system are exposed to high voltage slopes, parasitic capacitances may cause undesirable voltage ringing or non-uniform voltage distributions across the winding turns, with the consequence of increased stress on the transformer insulations. In [VIII], standardized analytical equations of parasitic inter and intra winding capacitances have been derived. Apart from minimizing the parasitic capacitances, an appropriate winding design should also eliminate the risk for electrical breakdown of the transformer insulation and keep the leakage inductance within a certain range suitable

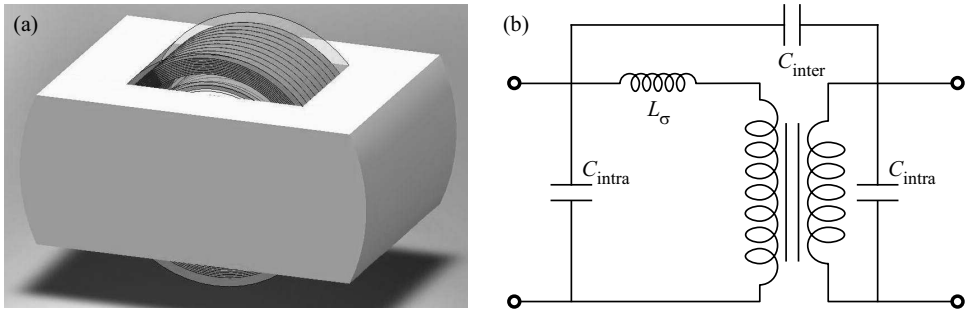

Figure 3.11: MF transformer design: (a) 3 MW single-phase shell-type design example, (b) Equivalent circuit including parasitic capacitances (ignoring winding resistances and assuming an ideal magnetic core).

for the cycloconverter phase leg commutations.

The design of MF transformers has been previously discussed, e.g. in [38], considering the frequency-dependency of winding, core, and dielectric losses. Compared to three-phase line-frequency transformers, single-phase MF transformers are cheaper, lighter, and more compact. In [VIII], a 3 MW distribution transformer operating at a frequency of 500 Hz was designed, see Fig. 3.11(a). Such a transformer has an efficiency of over 99.7 % and an active weight of approximately 2 metric tons. The design process in [VIII] has been especially adapted to the requirements of an application in an offshore wind farm. Using dry insulation is favorable due to environmental and safety aspects, but requires a thermal design adapted to the higher loss density in MF transformers. Since a transformer in a wind turbine is often operating below rated power, the relative importance of the core losses is higher than for the winding losses. Further details about the magnetic, electric, and thermal design of MF transformers, together with a reformulation of the modified Steinmetz equation based on the form factor of the voltage waveform can be found in [VIII].

The arrangement of the transformer windings determines the electrical parameters of the transformer, such as its leakage inductance and its parasitic capacitances, and thus its high-frequency behavior. In order to simulate the transient behavior of a transformer, both non-linearities and frequency dependencies must be taken into account. Since the interest lays on analysing the interaction of the transformer with the surrounding system, a terminal model seems to be most adequate. Transformer models in PSCAD consider hysteresis and saturation, but do not take the high-frequency behavior of the transformer into account. By including the parasitic capacitances, it should be possible to adequately characterize frequency components up to 100 kHz, including surge transfer [39]. Parasitic capacitances include primary and secondary intra winding capacitances, as well as the inter winding capacitance, which can be externally connected to the standard PSCAD single-phase transformer model for transient analyses, refer to Fig. 3.11(b).

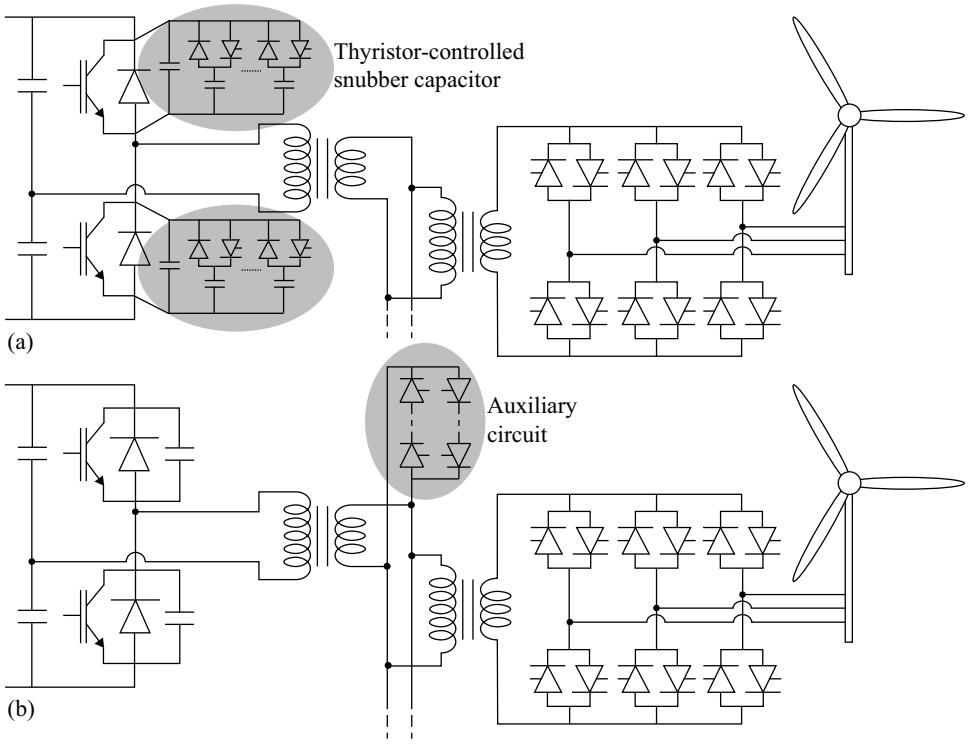

Figure 3.12: Solutions that enable the VSC commutation during low power generation: (a) Thyristor-controlled snubber capacitors, (b) Resonant commutation initiated by an auxiliary circuit.

3.2.3 VSC commutation during low power generation

An important objective of this work has been to investigate different possibilities of commutating the VSC during low power generation. According to (3.1), the duration of the VSC commutation t_{vsc} becomes unduly lengthy with a small transformer current i_{tr}, assuming a constant snubber capacitance C_s and DC-link voltage U_d.

$$t_{vsc} = 2 \cdot C_s \cdot \frac{U_d}{i_{tr}} \tag{3.1}$$

As a consequence, an alternative way of commutating the VSC has to be chosen whenever the transformer current drops below a certain value. Different alternatives to influence the duration of the VSC commutation are possible:

1. *Influence the snubber capacitance C_s:* Considering both mechanically and electronically controlled variable capacitors, thyristor-controlled snubber capacitors as shown in Fig. 3.12(a) look most promising for the intended application. Thyristor-controlled snubber capacitors can arbitrarily control the voltage slope during the VSC commutation, refer to Fig. 3.10(b), and hence the duration of the VSC commutation.

2. *Influence the transformer current i_{tr}:* Assuming fixed snubber capacitors, the only remaining possibility according to (3.1) is to influence the transformer current. Different solutions have been proposed:

   a) *Control strategy of the wind turbine induction generators:* By decreasing the stator voltage proportional to the frequency below nominal speed (maintaining nominal flux in the induction generator), a sufficient transformer current can be established with just a few wind turbines in operation. Such a control strategy causes the induction generators in the wind turbines to operate with a low power factor at low frequencies. For example, when a wind turbine after the start-up generates 4 % of the rated active power, the amplitude of the fundamental stator current already amounts to 0.38 p.u. (power factor of 0.13) [V]. The effect could be further increased depending on the chosen modulation strategy for the cycloconverters, refer to Fig. 5.6. This solution does not need any auxiliary ciruit, but considerably increases the losses during low power generation. To some extent, the voltage slope during the VSC commutation could be indirectly controlled by the cycloconverter modulation strategy and by adjusting the amplitude of the stator voltage of the wind turbine generators.

   b) *Resonant commutation:* The transformer current can be temporarily increased during the VSC commutation by a quasi-resonant commutation scheme.

      i. *Without auxiliary circuit:* It is possible to initiate a resonant process during the VSC commutation by short-circuiting the low voltage windings of all distribution transformers in the wind farm by means of the cycloconverters, as described in [IV,IX,X]. This resonant process can be utilized to recharge the snubber capacitors and is governed by the snubber capacitance and the equivalent inductance from the transformers and collection cables. The current increase allows a complete commutation of the VSC despite losses in the resonant circuit. However, such a resonant commutation scheme, which does not need any auxiliary circuit, would be difficult to implement as it requires a high level of coordination between the switchings of the VSC and the cycloconverters. This solution has originally been described in [11] and is verified both with simulations [24] and measurements [12].

      ii. *With auxiliary circuit:* Another possibility that reduces the extent of high-speed communication between the VSC and the cycloconverters is the installation of an auxiliary circuit as shown in Fig. 3.12(b), which was originally proposed in [24]. The auxiliary circuit initiates a resonant commutation in a similar way as described above, but involves only equipment that is installed besides the VSC [IV]. By placing the auxiliary circuit on the low-voltage side of the transmission transformer, fewer thyristors need to be series-connected.

When the transformer current is sufficiently high for a normal VSC commutation, the auxiliary circuit stays inactive.

In this section, different possibilities for commutating the VSC during low power generation have been proposed. Thyristor-controlled snubber capacitors, which are an original contribution, have the best characteristics and seem most suitable for the intended application of the MCC system. However, thyristor-controlled snubber capacitors add more complexity to the system and require a lot of auxiliary semiconductor devices. As a conclusion, the different proposed solutions, as well as combinations between them, should be evaluated regarding the equipment cost and the possibilities of controlling the VSC commutation duration. In addition, the losses during low power generation may be somewhat increased depending on the VSC commutation strategy.

3.2.4 Loss calculations

One of the contributions of this work has been to calculate the losses in MCC systems, both on a converter level [II] and a system level [III]. The converter losses are considerably reduced due to the soft-switching commutation scheme, which allows snubbered zero-voltage switchings of the VSC valves and natural commutations of the cycloconverter valves. In combination with a reduction of lossy components, such as the line-frequency transformers, a considerable decrease of the total losses may be achieved in MCC systems compared to conventional systems.

Paper [II] describes in detail how to calculate the conduction and switching losses in a VSC and in a cycloconverter. The pulse number (frequency modulation ratio) of the conventional three-phase hard-switching VSC is 19, which assures a similar effective switching frequency as in an MCC system operating at 500 Hz (where both the VSC and the cycloconverters mutually contribute to the effective switching frequency). The converter losses of a conventional VSC are based on and confirmed with measurements. In a wind farm with a rated active power of 200 MW, the switching losses are reduced by 81 %, the conduction losses by 44 %, and the total losses by 71 % in a single-phase soft-switched VSC compared to a conventional VSC, refer to Table 3.2.

Thyristors have very low switching losses compared to IGBTs. In a cycloconverter equipped with thyristors, the switching losses are reduced by over 93 % compared to a conventional full-size back-to-back VSC, refer to Table 3.2. Considering that a back-to-back VSC in a state-of-the-art doubly-fed induction generator (DFIG) is rated at approximately 10-15 % of the rated power, the switching loss reduction is still considerable. The conduction losses of a thyristor-based cycloconverter are comparably low, since only one of four thyristors per phase leg is conducting at a given instant. The conduction losses of a cycloconverter in an MCC system are approximately half the ones of a conventional full-size back-to-back VSC [II].

Table 3.2: Component losses at rated power: Comparison between an MCC system operating at 500 Hz and a conventional system with a three-phase VSC and a full-size back-to-back VSC (both operating with pulse number 19) [II,VIII].

	MCC system	Conventional system
VSC losses [kW]	825	2840
Switching losses [kW]	405	2092
Conduction losses [kW]	420	748
Cycloconverter losses [kW]	727	
Back-to-back VSC losses [kW]		3590
Switching losses [kW]	164	2560
Conduction losses [kW]	563	1030
Distribution transformer losses [kW]	449	2100

As discussed in Section 3.2.2, operating a transformer at medium frequency can considerably reduce the losses [VIII]. Looking at the losses of all distribution transformers in the wind farm, the reduction amounts to approximately 79 %, refer to Table 3.2. The loss reduction of the MF transmission transformer is expected to be less significant, since three-phase line-frequency transformers in the power range of 200 MW have a quite high efficiency of up to approximately 99.6 % [III].

Paper [III] presents a benchmark of the annual energy production of different converter systems for a wind farm rated at 200 MW. Two wind farm topologies with DFIG-equipped wind turbines and either HVAC or HVDC transmission system were compared with the proposed MCC system. Fig. 3.13 shows the combined wind farm and transmission system losses of the three topologies as a function of the transmission distance and the average wind speed, respectively. It can be concluded that the critical length for an HVAC transmission system, where the transmission losses are the same as for an HVDC transmission system, is reduced from over 100 km to approximately 80 km, see Fig. 3.13(a). This is due to the loss reduction in the MCC system by approximately 1 % of the annual energy production compared to conventional HVDC transmission systems. In addition, the MCC system has the lowest losses of all three considered topologies for transmission distances above 100 km independent of the average wind speed, see Fig. 3.13(b). Further details about the benchmark of the annual energy production for different wind farm topologies can be found in [III].

3.2.5 Economical aspects

In order to be able to compare different wind farm topologies on a fair basis, it is not sufficient to just consider the system losses. The most appropriate procedure

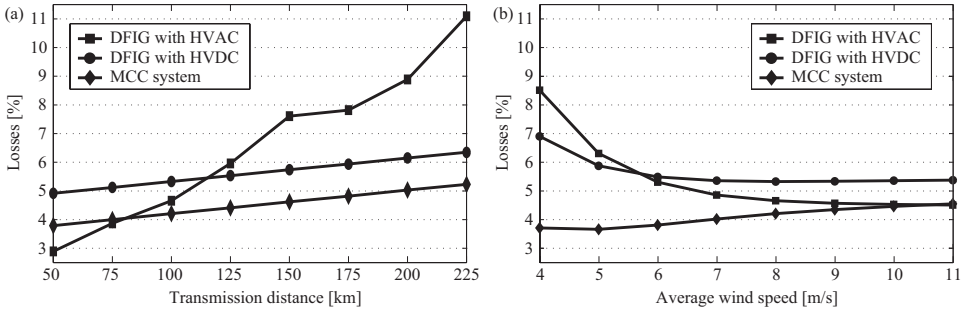

Figure 3.13: Combined wind farm and transmission system losses of three different topologies [III]: (a) as a function of the transmission distance at an average wind speed of 8 m/s, (b) as a function of the average wind speed with a transmission distance of 100 km.

Table 3.3: Characteristic figures indicating possible cost reductions of MCC systems [II,VIII].

	MCC system	Conventional system
Number of series-connected IGBTs in a 200 MW VSC	224 (one phase leg)	1440 (three phase legs)
Maximum IGBT voltage [kV]	5.2	2.5
Rated IGBT voltage [kV]	2.7	1.25
IGBT power rating of a 200 MW VSC [GW]	3.91 (500 Hz)	5.12 (pulse number 9) 5.69 (pulse number 19)
Active weight of a 3 MW distribution transformer [kg]	≈ 2000	≈ 7000

is to compare the effective energy generation cost, which apart from the losses also considers the initial equipment costs (neglecting currently not assessable factors such as the operation and maintenance costs, reliability issues, loss of production due to downtime, interest rates and economic depreciation of the investment, etc.). However, it is difficult to estimate the equipment costs, especially when it concerns a novel converter system which so far has not yet been constructed. However, the initial system cost strongly depends on the number of complex and expensive components, primarily the series-connected IGBTs in the VSC valves and the distribution transformers. Table 3.3 indicates that these components may have considerably lower initial costs in an MCC system compared to a conventional system.

Compared to a conventional hard-switched three-phase VSC, the proposed soft-switched single-phase VSC offers considerable advantages, even though the power rating of the converter remains unchanged. As a consequence of the reduction from three phase legs to a single phase leg, the IGBT power rating is reduced by at least 23 % (or more, depending on the pulse number), refer to Table 3.3. The reduction

to a single phase leg may also improve the reliability of the VSC.

The number of series-connected IGBTs, which are expensive and require complex gate drives and voltage-sharing circuitries, is also significantly reduced [II]. In addition, soft-switching with capacitive snubbers facilitates the voltage sharing between different IGBTs. Despite an increasing device current, the required active silicon area of the IGBTs in a 200 MW MCC system does not exceed the manufacturing limits of approximately 50 cm^2. Therefore, no parallel IGBTs are required. IGBTs in hard-switched applications are often thermally limited, i.e., the conduction and switching losses exceed the rated loss power density of the device. In a soft-switched application, the silicon area is often better utilized and the IGBTs are limited by the maximum turn-off current density of the device. As shown in Table 3.3, the reduction of the number of IGBTs is larger than an expected factor three, since the voltage rating of soft-switched IGBTs with 5.2 kV is higher than the 2.5 kV for hard-switched IGBTs. The higher voltage capability of soft-switched IGBTs can be explained by the snubbered commutation. The limited current slope capability and the consequently longer turn-off time allows in trade-off a higher blocking voltage capability, still with an acceptably low on-state voltage drop. In addition, the rated IGBT voltage in a snubbered application requires smaller margins for e.g. voltage spikes caused by diode reverse recovery currents, refer to Table 3.3.

Looking at the active weight of a 3 MW distribution transformer, it can be concluded that a weight reduction with over 70 % may result in cost reductions in the same range [VIII]. Other important factors contributing to the total system costs are the collection cables, where the three-phase cables are replaced by two single-phase cables, and the wind turbine converters. Cost estimations comparing a back-to-back VSC in a DFIG with a thyristor-based cycloconverter are out of the scope of this thesis. However, considering that thyristors are comparably cheap and reliable, it may not be a disadvantage to replace a state-of-the-art wind turbine converter with a full-size thyristor-based cycloconverter. In order to get more than just indications about economical aspects of MCC systems in a wind farm, more detailed investigations should be done.

3.3 Wind farm dimensioning proposal

One of the objectives of this work was to propose a feasible design of a wind farm based on an MCC system. As discussed in the previous sections, the most critical aspect is the design of the MF collection grid, which is distinct from previous applications of compact MCC systems. In [15], the influence of different parameters on the electromagnetic oscillations in the MF collection grid was investigated, namely the collection grid layout, the collection grid cable parameters, the voltage slope during the VSC commutation, and the electrical parameters of the MF transformers. In order to limit transient overvoltages on the collection grid, it is very important to be able to adjust the most critical design parameters. In Section 3.2.3, different

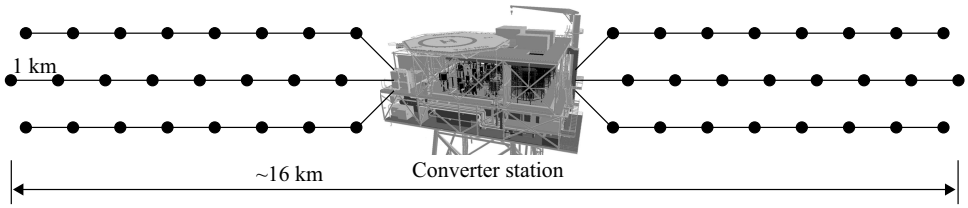

Figure 3.14: Example of a 144 MW wind farm layout consisting of 48 wind turbines rated at 3 MW each.

possibilities are described of how to control the voltage slope during the VSC commutation, with thyristor-controlled snubber capacitors according to Fig. 3.10 as the most promising alternative. In [VIII], it is described in detail how to influence the leakage inductance and the parasitic capacitances in MF transformers by changing the winding design.

Fig. 3.14 shows an example of how a feasible wind farm design could look like. With six cable feeders that each connect eight 3 MW wind turbines to a converter station, the rated power of the wind farm gets 144 MW. Since the frequencies of the resonances decrease for longer cables, the length of a cable feeder cannot be increased much more without causing extensive transient overvoltages on the MF collection grid. With a centrally locacted converter station, the maximum rated power of a wind farm based on a single MCC system is therefore limited. Such a wind farm has favorably a width of approximately 16 km perpendicular to the prevailing wind direction, and consists of three displaced rows of cable feeders as shown in Fig. 3.14.

Fig. 3.15 shows the no-load collection grid voltages at the wind turbine terminals, where the worst case originates from the wind turbines located farthest from the converter station, i.e., at a distance of 8 km. The peak overvoltage at these wind turbines amounts to approximately 30 %, while the transient overvoltages at the wind turbines closest to the converter station are below 10 %. Even though the VSC commutations occupy 18 % of the commutation cycle, the transient overvoltages are comparably high.

3.4 Conclusions

The application of an MCC system in a wind farm is possible, as shown in Section 3.3. However, some disadvantages arise when the converter system is distributed across a wind farm. Especially the long cables between the cycloconverters in the wind turbines and the VSC in the central converter station cause problems. In order to avoid extensive transient overvoltages, the duration of the VSC commutation has to be considerably prolonged. Consequently, the VSC commutation will occupy up to over 20 % of the commutation cycle with an operating frequency of 500 Hz. The voltage-time area lost during the VSC commutation considerably

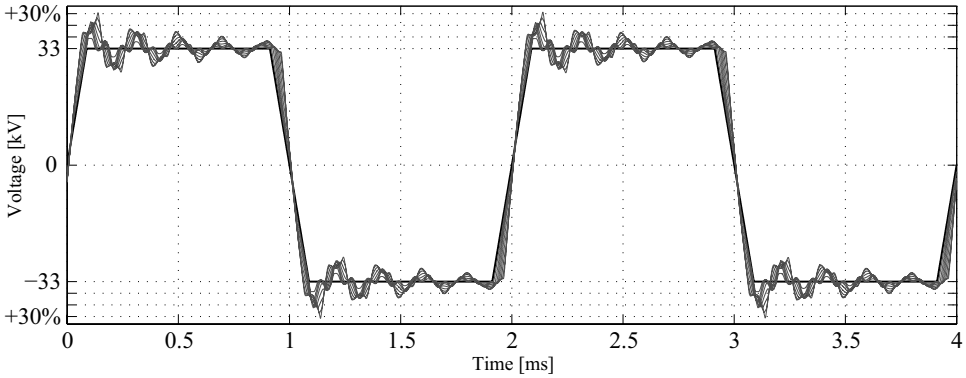

Figure 3.15: No-load collection grid voltages at the wind turbine terminals along an 8 km long cable feeder.

reduces the maximum possible modulation ratio and results in unintentional power pulsations on the collection grid. As a consequence of the low utilization of the commutation cycle, the rating of the converter system increases unnecessarily.

A feasible solution that results in a lower percentage of lost commutation time with the same voltage slope is to reduce the operating frequency. A reduction of the operating frequency by 50 % to 250 Hz would require some adjustments of the converter system. For example, the lower the operating frequency, the smaller the advantage of the MF transformers. In order to get a suitable modulation of the output voltages, the frequency modulation ratio of the cycloconverters cannot be further decreased. Therefore, the frequency of the wind turbine generators should be reduced accordingly (i.e., from 50 Hz to 25 Hz). A squirrel-cage induction generator can be operated down to approximately 20 Hz without any problems. The output filter of the cycloconverters should also be adjusted accordingly. Decreasing the switching frequency by 50 % probably moves critical low-order harmonics away from system resonances, thus allowing the voltage rise time to be increased.

Finally, it should be investigated whether or not it may be more beneficial to remove critical voltage harmonics with filters rather than to reduce the voltage slope during the VSC commutation. Such filters may be very advantageous, since they may reduce the need to overrate the equipment for the transient overvoltages on the collection grid.

4 Modulation methods

Apart from providing the desired voltage waveform, a suitable modulation method should also have a high maximum modulation ratio and reduce the harmonic content in the output voltage. This chapter gives an overview and comparison of different modulation methods for MCC systems, which have comparably restrictive modulation conditions. Finally, a modulation method is proposed that does not require any turn-off capability in the cycloconverter valves.

4.1 Modulation constraints of mutually commutated converter systems

In Section 3.1 it was shown that it is possible to maintain soft-switching conditions for all semiconductor devices by consistently commutating the VSC and the cycloconverter in alternation. This implies that one of the edges of each voltage pulse is due to the switching action of the VSC. The other edge of the voltage pulse may be arbitrarily placed in the interval between two VSC switching instants by commutating the corresponding cycloconverter phase leg. With this in mind, two main modulation constraints regarding the possibilities for modulating the AC-side voltages arise:

1) The VSC should be commutated with a constant frequency in order to generate an MF transformer voltage without low-frequency or DC components. As a consequence, one of the slopes of each voltage pulse occurs at a constant interval. This corresponds to a carrier-based modulation method with sawtooth carrier, where the carrier frequency equals twice the transformer frequency [24].

2) In order to be able to naturally commutate the cycloconverter phase legs, the sign of each phase voltage has to be opposite to the sign of the corresponding line current after a VSC commutation. This implies that the instantaneous direction of the line current determines if the pulse will be of the type $low \rightarrow high$ with the leading edge modulated (for positive current directed out of the phase outlet) or of the type $high \rightarrow low$ with the trailing edge modulated (for negative current directed into the phase outlet) [24]. Consequently, the type of pulses has to be altered twice every fundamental period for each cycloconverter phase leg.

4.2 Sinusoidal pulse width modulation

Essentially, sinusoidal PWM (SPWM) attempts to synthesize a sine-wave output by a series of width-modulated pulses, determined by the instantaneous intersections between a sinusoidal reference wave and a carrier wave [40, 41]. The carrier is typically a triangular or sawtooth waveform with a frequency that is considerably higher than that of the reference waveform. The ratio between carrier and reference frequency equals the number of pulses per fundamental cycle and is therefore called *pulse number* or *frequency modulation ratio*.

The *amplitude modulation ratio* is defined as the ratio between the amplitude of the reference waveform and the carrier amplitude [31]. The maximum possible *modulation ratio* (amplitude of the normalized fundamental-frequency component in the output voltage) for SPWM under idealized conditions is 1.0 in the linear region, i.e., the reference waveform never exceeds the amplitude of the carrier. When the reference waveform is further increased, so called *overmodulation*, the maximum possible modulation ratio can be extended up to 1.28 ($= 4/\pi$), corresponding to a square-wave output voltage. During overmodulation, however, the modulation ratio does no longer vary linearly with the amplitude modulation ratio as in the linear region. The output voltage also contains a considerable number of additional harmonics in the sidebands [31].

SPWM with sawtooth carriers [11, 42] is a simple and straightforward solution that can cope with the modulation constraints of MCC systems described in Section 4.1. Fig. 4.1(a) illustrates how the switching instants for the cycloconverter phase legs are determined by the comparison of the reference phase voltages u^* with two repetitive sawtooth carriers. In order to be able to naturally commutate a cycloconverter phase leg, the sign of each phase voltage has to be opposite to the sign of the corresponding line current prior to the cycloconverter commutation. This implies that the slope of the carrier is either positive or negative, depending on the direction of the current in the respective cycloconverter phase leg. Furthermore, before a subsequent VSC commutation, the sign of each phase voltage should correspond to the sign of the corresponding line current. If this is not the case, i.e., one of the currents changed sign during the commutation interval, the corresponding phase leg has to be recommutated.

4.3 Space vector modulation

SVM has gained great popularity as it is relatively simple to implement digitally and inherently compatible with modern current and torque control schemes. For MCC systems, a space vector representation simplifies the analysis of the different constraints and possibilities for the modulation of the cycloconverter. Equation (4.1) describes how the three-phase quantities are transformed into their space vector

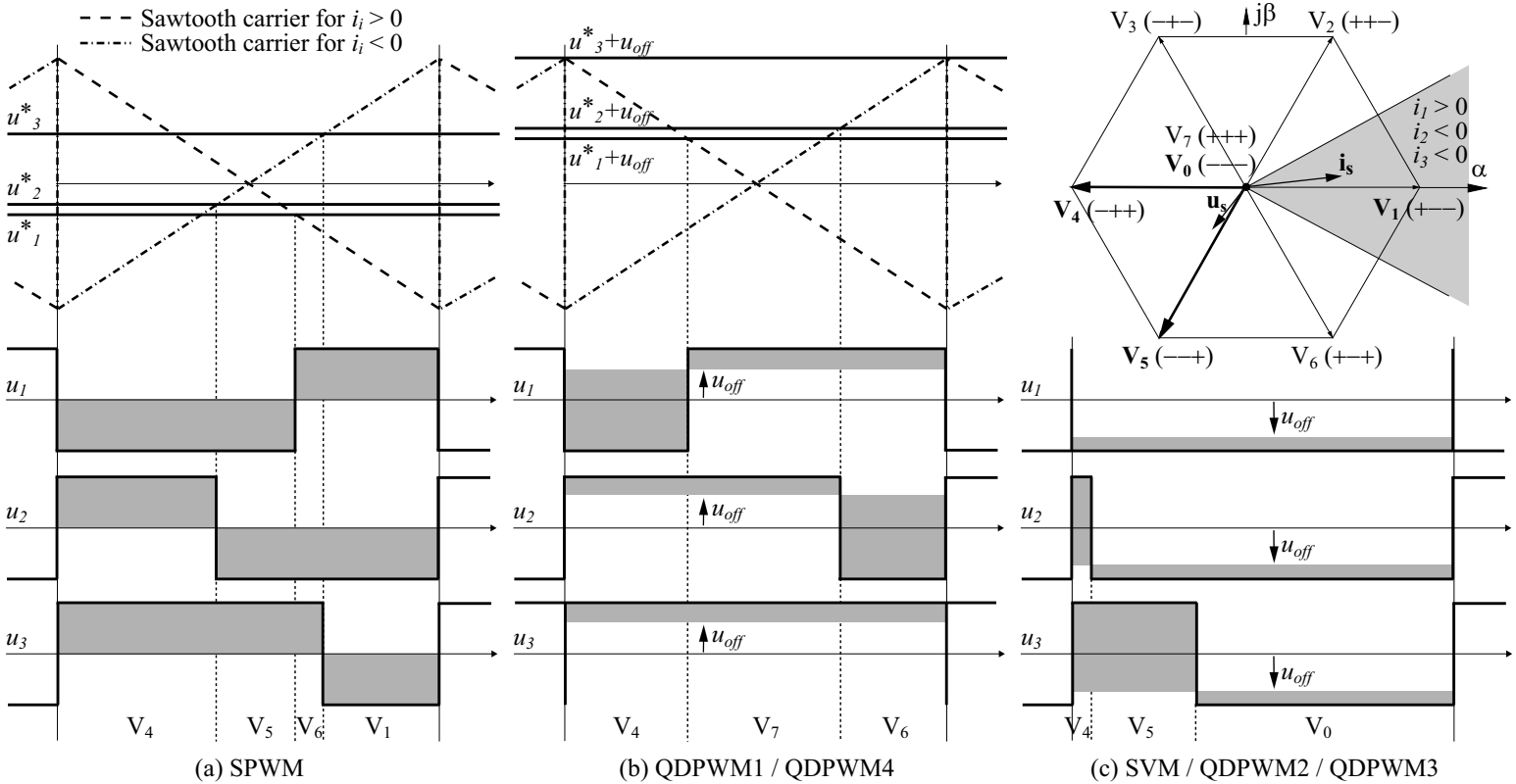

Figure 4.1: Comparison of different modulation methods during one modulation interval.

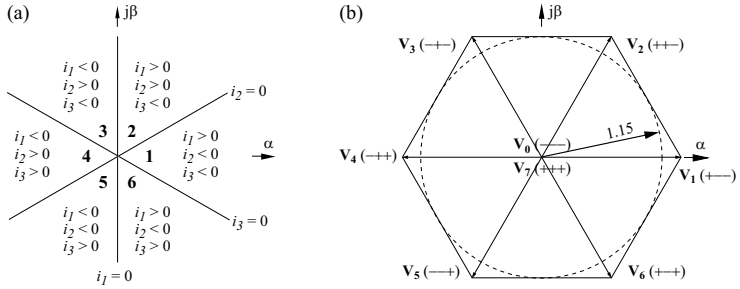

Figure 4.2: Space vector modulation: (a) Current sectors, (b) Base voltage vectors.

equivalents:

$$\begin{pmatrix} i_{s\alpha} \\ i_{s\beta} \end{pmatrix} = \begin{pmatrix} \frac{2}{3} & -\frac{1}{3} & -\frac{1}{3} \\ 0 & \frac{1}{\sqrt{3}} & -\frac{1}{\sqrt{3}} \end{pmatrix} \cdot \begin{pmatrix} i_1 \\ i_2 \\ i_3 \end{pmatrix} \tag{4.1}$$

Fig. 4.2 shows that the actual direction of the three line currents defines six different current sectors. It is also shown that the voltage space vectors corresponding to the switching states of the cycloconverter (base vectors) form a hexagon, with two zero voltage vectors in its center, where all the phase legs are connected to the same DC-link terminal. As illustrated in Fig. 4.2(b), the modulation ratio for SVM is extended up to 1.15 ($= 2/\sqrt{3}$) in the linear region.

In SVM for conventional VSCs, a modulation interval is always starting with a zero vector and ending with the opposite zero vector. The switching sequence is chosen such that the active base vectors are the ones adjacent to the reference voltage vector. The switching instants are determined such that the vectorial time-average of the base vectors during the modulation interval corresponds to the reference voltage vector.

The modulation constraints of an MCC system differ from those of a conventional VSC in several aspects, see Section 4.1. In order to allow the cycloconverter phase legs to be naturally commutated, the sign of each phase voltage has to be opposite to the sign of the corresponding line current after the VSC commutation. This implies that the modulation interval begins with an active voltage vector opposite to the instantaneous direction of the current vector and ends with the voltage vector of opposite direction (unless one of the line currents is changing sign). Fig. 4.3 shows all possible base-vector sequences for the case where the current vector is located in the first sector. Every cycloconverter phase-leg commutation corresponds to a transition along one of the segments in the voltage hexagon. The vector sequences consist of four base vectors. In practice, either the first or last base vector is suppressed (moved to the immediate beginning or end of the modulation interval), such that a three-vector sequence is obtained. Consequently, voltage vectors of opposing direction can be avoided during the same modulation interval, which reduces unnecessary power pulsations.

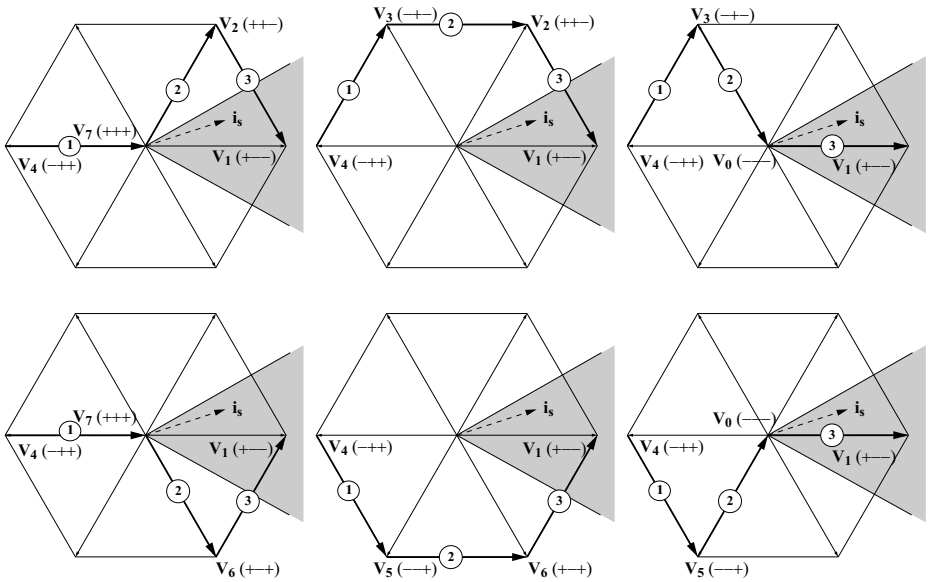

Figure 4.3: Possible base-vector sequences with the current vector located in the first sector.

Suitable SVM methods for MCC systems have been previously described, at first only for low values of the load angle [43], but then as well for the general case [44]. The latter has been adapted from a modulation method originally developed for quasi-resonant DC-link converters, which have similar modulation constraints as MCC systems [45]. The SVM method described in [44] offers a systematic approach on how to choose the vector sequence for a modulation interval, based on information about the line currents and the desired reference voltage vector (refer to Fig. 5.4). The functional principle of this SVM method is illustrated in Fig. 4.4. The problem is reduced to the case where the current vector is located in the first sector. Depending on the actual current-direction region k, the reference voltage vector $\mathbf{u_{ref}}$ is transformed in such a way that it corresponds to the case where the current vector would be located in the first sector. At the end of the procedure, the calculated base vectors are reverse transformated accordingly.

The main task of the SVM method is to identify a suitable vector sequence and to calculate the duty cycle, i.e., the durations of the calculated base vectors, refer to Fig. 4.1(c) for an example. The choice of vector sequence depends on where the transformed reference voltage vector $\mathbf{u'_{ref}}$ is located. For load angles around 0° and 180° (regions A, D, E and H in Fig. 4.4), a sequence of two adjacent base vectors and a zero vector can be used. For load angles around 90° and 270°, the choice of vector sequence becomes more complex. In the regions B1, C1, F1, and G1, combinations of two non-adjacent vectors and a zero vector are possible. The regions B2, C2, F2, and G2, however, can only be reached by a sequence consisting of three adjacent vectors. Such a choice of vector sequence ensures that the zero

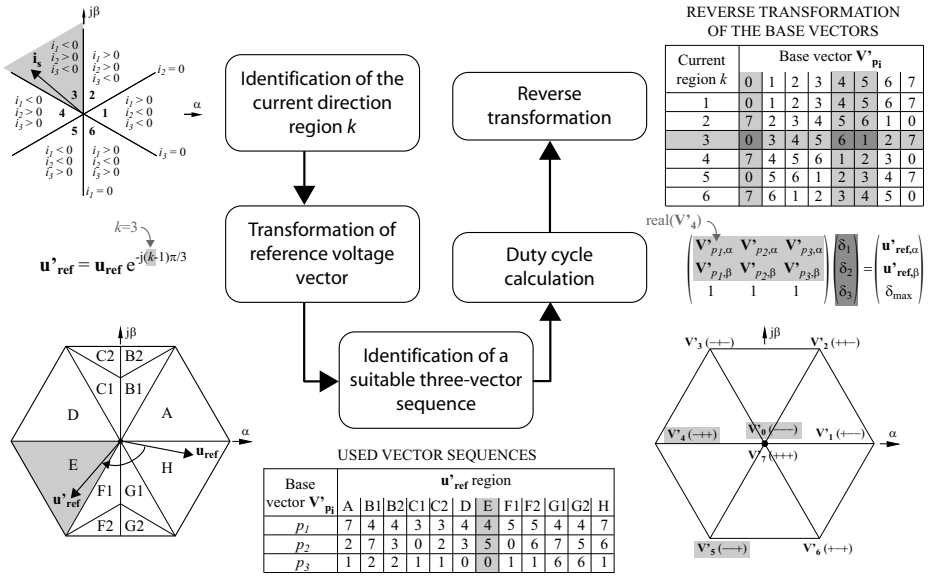

Current region k	Base vector $\mathbf{V'}_{p_i}$							
	0	1	2	3	4	5	6	7
1	0	1	2	3	4	5	6	7
2	7	2	3	4	5	6	1	0
3	0	3	4	5	6	1	2	7
4	7	4	5	6	1	2	3	0
5	0	5	6	1	2	3	4	7
6	7	6	1	2	3	4	5	0

Base vector $\mathbf{V'}_{p_i}$	$\mathbf{u'}_{ref}$ region										
	A	B1	B2	C1	C2	D	E	F1	F2	G1	G2	H
p_1	7	4	4	3	3	4	4	5	5	4	4	7
p_2	2	7	3	0	2	3	5	0	6	7	5	6
p_3	1	2	2	1	1	0	0	1	1	6	6	1

Figure 4.4: SVM method for choosing the vector sequence during one modulation interval [VI].

vectors are maximized, which reduces unnecessary internal power pulsations along with related power losses.

4.4 Quasi-discontinuous pulse width modulation

The SVM method proposed in [44] and introduced in Section 4.3 consistently generates three-vector sequences with a maximized zero vector. The three-vector sequences are obtained as subsets of the basic four-vector sequences by suppressing one of the base vectors, i.e., one of the cycloconverter phase-leg commutations will occur either immediately before or after the VSC commutation. The same effect can be obtained by adding a zero-sequence component u_{off} to the sinusoidal PWM reference waveforms. Thereby, one of the reference waveforms will be temporarily fixed to one of the DC-link terminals, either the upper as in Fig. 4.1(b) or the lower as in Fig. 4.1(c). Even though the switching of the concerned cycloconverter phase leg will not cease, in practice it will be effectively clamped to the concerned DC-link terminal, which explains the name quasi-discontinuous PWM.

The addition of a zero-sequence component to the reference waveforms represents an important degree of freedom that can be used for many purposes, e.g. harmonic elimination or extension of the linear modulation region up to 1.15 ($= 2/\sqrt{3}$ as for SVM). Fig. 4.5 shows different relevant clamping strategies and Table 4.1 gives the equations for calculating the zero-sequence component u_{off} from the three voltage reference waveforms.

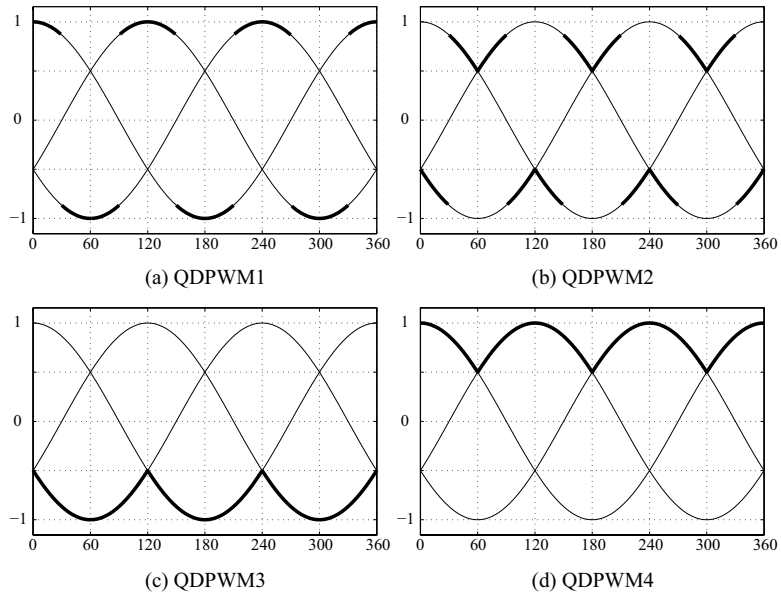

Figure 4.5: Clamped waveform sections for QDPWM: (a) QDPWM1 (clamp at voltage peaks), (b) QDPWM2 (clamp opposite to voltage peaks), (c) QDPWM3 (clamp to lower DC-link terminal), (d) QDPWM4 (clamp to upper DC-link terminal).

Table 4.1: Equations for calculating the zero-sequence component u_{off} for the clamping strategies shown in Fig. 4.5.

QDPWM1	$(1 - \max(\lvert u_1^* \rvert, \lvert u_2^* \rvert, \lvert u_3^* \rvert)) \cdot \text{sign}(u_1^* \cdot u_2^* \cdot u_3^*)$
QDPWM2	$-\max\left(1 - \max(u_1^*, u_2^*, u_3^*), 1 + \min(u_1^*, u_2^*, u_3^*)\right) \cdot \text{sign}(u_1^* \cdot u_2^* \cdot u_3^*)$
QDPWM3	$-\left(1 + \min(u_1^*, u_2^*, u_3^*)\right)$
QDPWM4	$1 - \max(u_1^*, u_2^*, u_3^*)$

According to Holmes and Lipo [46], discontinuous PWM is often the most effective way to implement digital SVM control. Fig. 4.6 shows which three-vector sequences that are used in different voltage regions for the four investigated QDPWM methods, assuming that the current vector is located in the first sector. Those voltage sectors that use the same optimum vector sequence as SVM are highlighted in grey. Compared to SVM, clamping the phase with the largest reference magnitude (QDPWM1) only results in identical pulse patterns for load angles that are 0° and 180°, refer to Fig. 4.6. However, Table 4.2 shows that it is possible for all load angles to choose a suitable QDPWM strategy that produces the same pulse patterns as SVM.

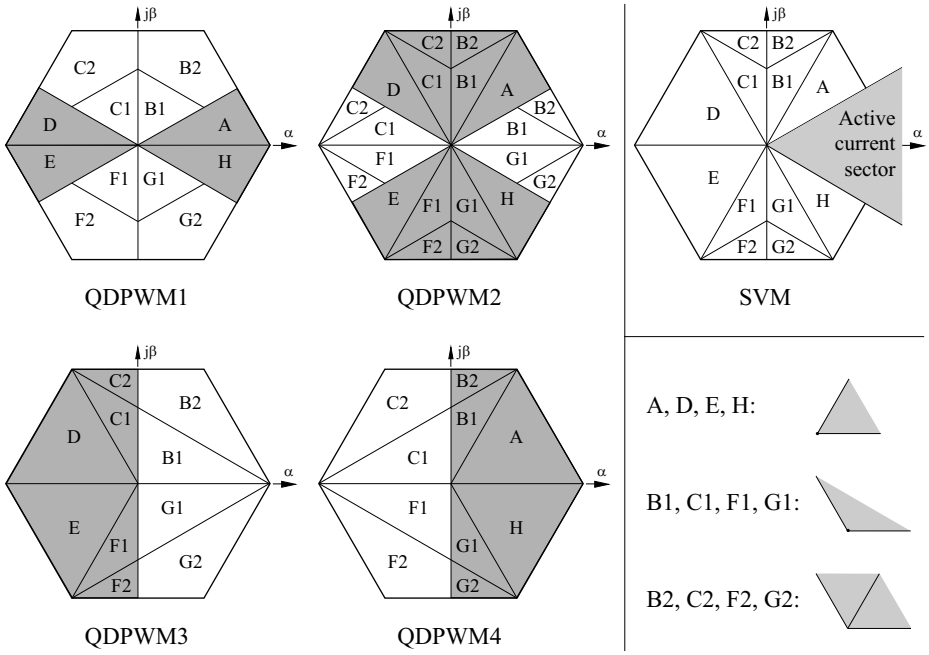

Figure 4.6: Voltage regions classified by the principle three-vector sequences used (sectors corresponding with SVM are highlighted in grey).

Table 4.2: Load angle dependent choice of QDPWM strategy that corresponds with SVM.

Load angle:	QDPWM strategy:
0° - 60°	QDPWM4
60° - 120°	QDPWM2
120° - 240°	QDPWM3
240° - 300°	QDPWM2
300° - 360°	QDPWM4

4.5 Space vector modulation for thyristor-based cycloconverters

Thyristors are often prefered to other switching devices due to the low conduction losses at high current levels and due to the unsurpassed robustness and reliability. In MCC systems it is often possible to utilize thyristors, since the VSC and the cycloconverter are alternately commutated, which reduces the effective switching frequency and allows the cycloconverter valves to be naturally commutated. As a consequence, the cycloconverter valves do not need any turn-off capability and the IGBTs can be replaced by fast thyristors in order to gain the full benefits of

MCC systems. In this section, the detailed theory behind SVM for thyristor-based cycloconverters in MCC systems is described.

4.5.1 Additional modulation constraints and their significance

Utilizing thyristors in the cycloconverter imposes additional constraints on the modulation strategy in addition to those of conventional MCC systems described in Section 4.1. Therefore, the proposed modulation strategies in the previous sections are not suitable and adapted for cycloconverters equipped with thyristors and have to be modified in order to comply with:

1) *Absence of turn-off capability:* Thyristors cannot be switched off from the gate. It is only possible to turn off a thyristor when its anode current tries to go negative under the influence of the external circuit. Since the cycloconverter phase legs are naturally commutated, this is normally the case. However, if one of the line currents changes sign, the conditions for a natural commutation are no longer fulfilled in the respective cycloconverter phase leg.

2) *Thyristor turn-off time:* After turning off a thyristor, it must be reverse-biased for a certain duration (thyristor turn-off time t_q) before a positive voltage can be reapplied. If a thyristor gets forward biased before the turn-off time t_q has elapsed, it may unintentionally be self-triggered, which is often destructive.

The second constraint above is associated with the timing of the commutation scheme and can be coped with relatively easy. In practice, it implies that the last base vector in every modulation interval has to be maintained during at least the time t_q in order to prevent the thyristors from accidentally turning on during the subsequent VSC commutation. This is especially critical for MCC systems where the power flow is directed from the AC side to the DC side, which signifies that the commutation instants are located towards the end of the modulation interval. In order to avoid any problems, a safety margin corresponding to t_q should be kept at the end of the modulation interval during which no cycloconverter phase leg commutations are allowed. However, since the last base vector will always be present during the time t_q, this has to be balanced by also applying the first base vector for the same duration (see Fig. 5.12). This reduces somewhat the maximum possible modulation ratio at the same time as it slightly increases the current ripple.

The absence of turn-off capability appears to be an even greater limitation for the operation of the cycloconverter, especially when the current vector moves out of the initial sector during a modulation interval (i.e., one of the line currents changes sign). If the phase leg commutation appears prior to the current sign reversal, see Fig. 4.7(a), the subsequent zero current crossing re-establishes the conditions for another natural commutation of the corresponding cycloconverter phase leg, which makes an extra re-commutation at the end of the modulation interval possible [VII].

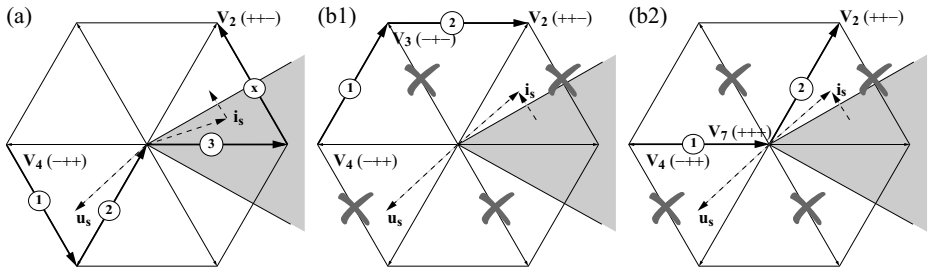

Figure 4.7: Base-vector sequences when the current is moving from the first into the second sector: (a) Phase leg commutation prior to current sign reversal (requires extra commutation), (b) Current sign reversal before intended phase leg commutation.

However, if the current sign reversal appears prior to the phase leg commutation, a natural commutation of the corresponding phase leg is no longer possible and one of the directions in the voltage hexagon will be inhibited, see Fig. 4.7(b). Therefore, the desired base vector sequence is no longer possible. From the two possible vector sequences, refer to Fig. 4.7(b), the latter (b2) is the most attractive with regard to the given voltage reference vector, even if it cannot provide the desired pulse pattern during the actual modulation interval. However, both vector sequences in Fig. 4.7(b) have the advantage that an additional phase leg commutation at the end of the modulation interval can be avoided.

4.5.2 Current-clamping control strategy

In order to ensure that the cycloconverter can be commutated satisfactorily despite the limited controllability of the thyristor valves, a new modulation strategy is required whenever one of the line currents approaches zero. Previously proposed solutions, such as the dead-time control strategy [47], where the gate pulses to the thyristors are simply stopped for a constant time period if the output current is lower than a certain threshold value, are not suitable in the considered application [VII]. The proposed current-clamping control strategy is instead stopping the gate pulses in the phase leg where the current is close to zero for a controlled time period during every modulation interval [V].

The current-clamping control strategy determines the initial base vector sequence and the commutation instants according to the SVM strategy shown in Fig. 4.4. Then, a current predictor determines the trajectory of the current vector for the calculated base vector sequence, in order to predict in advance if and exactly when the current vector will leave the initial sector. In case of an imminent change of current sector, there is enough time to alter the base vector sequence accordingly (refer to Fig. 5.12).

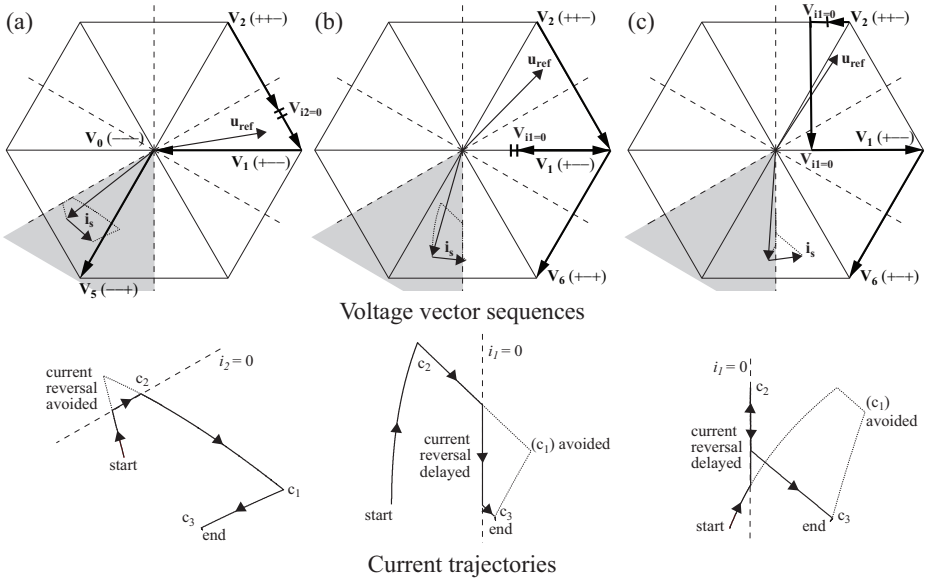

Figure 4.8: Examples of base-vector sequences and corresponding current trajectories with current-clamping control strategy (the current vector is initially located in the fifth sector).

If the current trajectory is only temporarily leaving the initial current sector during a modulation interval as for instance in Fig. 4.8(a), a zero current transition should be avoided. This is done by not gating on the anti-parallel thyristor in the conducting valve of the corresponding phase leg. This implies that the line current through the initially conducting device is turned off once it gets zero and the phase outlet is getting isolated from the DC-link terminals. By correctly choosing the commutation instant of the corresponding phase leg, it is still possible to provide the desired reference voltage during this modulation interval. In the example in Fig. 4.8(a), which is the most common and basic case, the commutation of the second phase leg (c_2) is delayed to the instant when the current would originally have re-entered the initial current sector.

Fig. 4.8(b,c) shows two different examples where the current vector is actually required to change into a neighboring current sector. In this case it is not possible to maintain the desired voltage sequence in a conventional manner due to the fact that the phase leg in which the current is changing sign can either not at all be commutated or not at the desired instant. The proposed current-clamping control strategy compensates this drawback by controlling the dead-time during which the corresponding line current is kept to zero. Once the anti-parallel thyristor to the previously conducting thyristor in the same cycloconverter valve is gated on, the current will start flowing into the new current sector. In this way the control over the phase leg in which the current is changing sign can be regained. Therefore, it is possible to provide the desired reference voltage during every single modulation

interval. The example in Fig. 4.8(c) differs from the case in Fig. 4.8(b) in the way that a commutation takes place in another phase leg while the current is clamped.

Fig. 4.8 shows also the voltage vector sequences, which now contain voltage vectors during the current clamping that differ from the eight base vectors. Therefore, it is not trivial to determine the exact timing for the phase leg commutations and the release of the current clamping. The switching instants have to be determined prior to the start of the modulation interval by means of a current predictor.

4.6 Conclusions

In this chapter, different modulation strategies for MCC systems have been discussed, such as PWM, SVM, and QDPWM. It has been shown that it is always possible to choose a suitable QDPWM strategy that produces the same pulse patterns as SVM. In addition, a current-clamping control strategy has been proposed that allows to replace the IGBTs in the cycloconverter with thyristors. Despite the reduced controllability of thyristors, the current-clamping control strategy can provide the desired reference voltage during every single modulation interval. Table 4.3 provides some references about different modulation strategies, primarily regarding MCC systems.

All discussed modulation strategies in this chapter have the drawback that they just consider a single modulation period. Due to the characteristics of MCC systems, the type of pulses has to be altered twice every fundamental period. This implies that the moving average of the phase voltage diverges from its reference value during the zero current crossing, even though the average phase voltage is correct both during the precedent and the subsequent modulation period. As a consequence, the line current gets distorted during the zero current crossing, which results in low-order harmonics. The proposed current-clamping control strategy further deteriorates the harmonic properties [13] by clamping the current before its zero crossing.

It should be investigated if a trajectory tracking approach, which would either control the current trajectory [48] or the stator flux trajectory [49] could mitigate the current distortion during zero current crossings.

Table 4.3: Further reading.

SPWM	
[31] (p. 200 ff.)	General textbook description.
[40, 41]	Original references.
[11, 12, 24, 42] [I,IV,IX,X]	Application to MCC systems.
[44]	Evaluation of output voltage harmonic distortion and RMS transformer current.
QDPWM	
[46] (p. 299 ff.)	General textbook description.
[44]	Evaluation of output voltage harmonic distortion and RMS transformer current (QDPWM1).
SVM	
[46] (p. 24 ff.)	General textbook description.
[43, 44]	Original references of SVM for MCC systems.
[44]	Evaluation of output voltage harmonic distortion and RMS transformer current.
[VI]	Experimental implementation and measurement results.
SVM with current-clamping control strategy	
[V]	Original description and simulation results.
[13]	Evaluation of output voltage harmonic distortion and cascaded MCC systems.
[VII]	Experimental implementation and measurement results.

5 Experimental activities

The practical implementation of the different modulation methods for MCC systems presented in Chapter 4 was an important part of this project. The experimental activities have been focusing on a first converter system with an IGBT-based cycloconverter (Prototype I) and a second converter system with a thyristor-based cycloconverter (Prototype II). In this chapter, the two prototype converter systems, their control hardware, and the implementation of the SVM and current-clamping control strategy are described in detail. Finally, the most important experimental results are presented and evaluated.

5.1 Prototype I with IGBT-based cycloconverter

Dr. Staffan Norrga designed and built up *Prototype I*, see Fig. 5.1. A detailed description of the main circuit, the gate drive units, and the control system of *Prototype I* can be found in [12, 24]. These two references also provide measured characteristic voltage and current waveforms, as well as overall system efficiency and harmonic spectrum measurements under different operating conditions using SPWM. In this section, *Prototype I* is briefly introduced before focusing on work done during this project, i.e., the implementation and evaluation of SVM.

The rated power of *Prototype I* is approximately 40 kVA and it operates with a DC-link voltage of 600 V. The operating frequency of the MF transformer is 6 kHz. Further relevant prototype parameters can be found in Table 5.1. In the experimen-

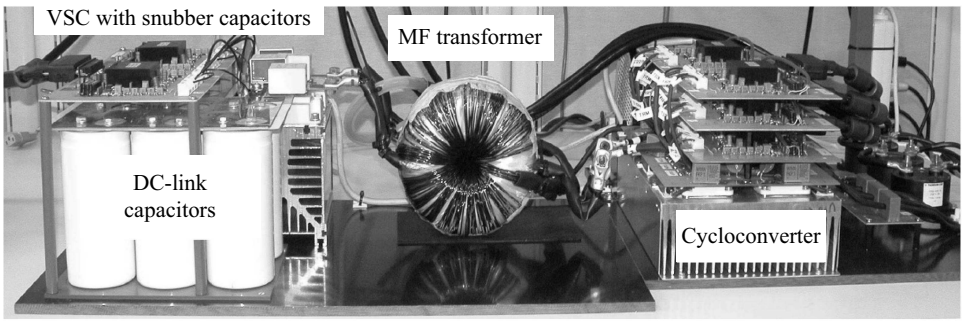

Figure 5.1: Photograph of *Prototype I*.

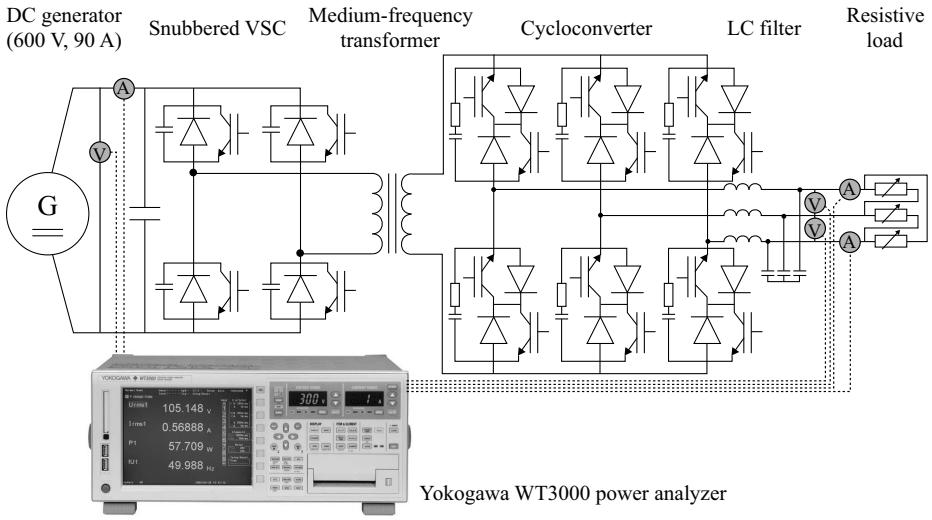

Figure 5.2: Schematic of *Prototype I*, setup for efficiency measurements.

Table 5.1: Parameters of *Prototype I*.

Rated power	40 kVA
DC-link voltage	600 V
DC-link capacitance	2.9 mF
VSC snubber capacitance, per valve	0.1 μF
Transformer operating frequency	6 kHz
Transformer turns ratio	1:1
Transformer leakage inductance	2.3 μH
Cycloconverter RC-snubbers	50 Ω / 15 nF
AC-side filter inductors	1.2 mH
AC-side filter capacitors (Y-connected)	33 μF

tal setup, the VSC was connected to a DC generator and the cycloconverter to a variable resistive load, via an LC-filter, see Fig. 5.2. The inductive filter on the AC side allows to control the power flow, which was directed from the DC to the AC side. It should be mentioned that the cycloconverter valves are equipped with small RC-snubbers for overvoltage protection during diode reverse recovery. More details about the implementation of the cycloconverter and VSC valves as well as the MF transformer can be found in [IX, X]. Since the control system for *Prototype I* is the same as for *Prototype II*, a short summary is presented below.

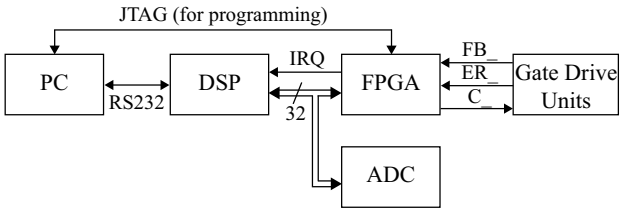

Figure 5.3: Control hardware overview.

5.1.1 Control system

The digital control functions in the system are shared between a digital signal processor (DSP) which performs computational tasks and a field-programmable gate array (FPGA) which handles logic functions that have to be executed with low latency [24]. These two devices are coupled by the external bus of the 32-bit floating-point DSP, see Fig. 5.3.

The DSP (Analog Devices 21065L) is basically a processor that sequentially executes programming code, which makes it useful for computational tasks. Once every commutation cycle, initiated by an interrupt from the FPGA, it computes the switching instants for the following commutation cycle and evaluates the analogue inputs. These analogue inputs are the three line currents and the DC-link voltage, which are measured by Hall-element based voltage and current sensors, whose outputs are sampled by A/D converters (ADC) that can be accessed from the DSP bus. The DSP monitors possible over- and undervoltages on the DC side and overcurrents on the AC side, in order to protect the prototype converter. The DSP also handles the communication with a PC via an RS232 link, see Fig. 5.3.

The FPGA (Xilinx Virtex XCV200) is a programmable logic circuit, which holds most of the key control functions in the system, such as the timing and control of the commutation processes [12]. A description of the FPGA development and debugging environment can be found in [24]. The control algorithms are basically realized with a set of coupled finite state machines embedded in the FPGA. Since the commutation instants of the cycloconverter phase legs depend on the respective current sign, the current sensors are also directly connected to the FPGA via fast comparators, in order to create digital signals with low latency indicating the direction of the line currents. In addition, the commutations of the VSC and the cycloconverter (digital signals 'C_') must be precisely coordinated. Therefore, it is desirable to be able to rapidly detect the switching states of the converter valves. This is realized by feeding information about the voltage across each converter valve back to the FPGA (digital signals 'FB_'). The gate drive units are also designed to detect fault conditions from both the VSC and cycloconverter valves (digital signals 'ER_'). Whenever a fault condition appears, the prototype converter is immediately shut down by turning off all VSC valves and short-circuiting all cycloconverter valves [24].

A more detailed description as well as a functional overview of the control system can be found in [24]. It should also be mentioned that no closed-loop control was implemented. Instead, the DSP was directly generating sinusoidal voltage references with the desired frequency and magnitude.

5.1.2 Implementation of space vector modulation

One of the objectives of this project was to practically implement SVM in *Prototype I*. This implementation is described in detail in [VI] and is a prerequisite for the implementation of the current-clamping control strategy described in Section 5.2.3. The software implementation of the SVM method shown in Fig. 4.4 mainly differs from previously described carrier-based modulation methods in how the switching instants for the three cycloconverter phase legs are calculated in the DSP.

Fig. 5.4 shows a time diagram over two consecutive commutation cycles in order to clarify the implementation of SVM. Once every commutation cycle, the FPGA alerts the DSP via an interrupt ('IRQ') to calculate a new set of control signals and timing intervals. However, since the current sector at the beginning of the next commutation cycle is still unknown, the cycloconverter phase leg switching instants are calculated for all six possibilities, see Fig. 5.4. After the sampling of the current directions at the beginning of the commutation cycle, the FPGA decides which switching instants that should be used. In case that a line current changes sign prior to the commutation of the respective phase leg, the conditions for a soft commutation are no longer given. However, the resulting hard switching is not critical, neither in terms of losses nor in terms of stress on the valve, since such a commutation occurs at a very low current magnitude and at most a few times per fundamental cycle.

Another characteristic of modulation methods suitable for MCC systems is the necessity of establishing soft-switching conditions at the end of each commutation cycle. For example, a sign reversal of one of the line currents implies that the condition for the respective phase leg is no longer fulfilled. A power reversal check of all cycloconverter phase legs at the end of the commutation cycle ensures that soft-switching conditions are re-established if necessary. During the time interval t_{prc}, additional cycloconverter phase leg commutations (under soft-switching conditions) are still possible.

5.1.3 Measurement results

During this project, various measurements have been performed on *Prototype I*, both under operation with SPWM [VI,IX,X] and SVM [VI]. These measurements comprise voltage and current waveforms, frequency spectrum, transformer current,

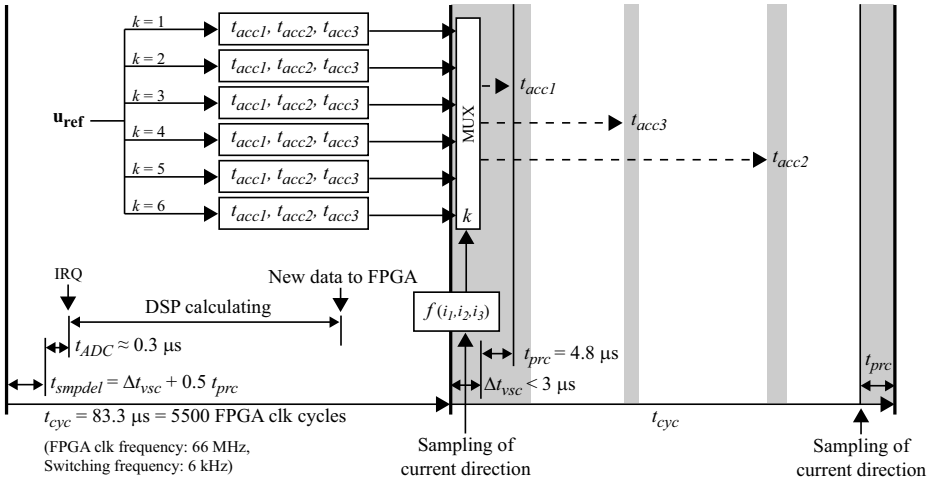

Figure 5.4: Implementation of SVM in *Prototype I*: Time diagram over two consecutive commutation cycles [VI].

Table 5.2: Measurement equipment.

Measurement:	**Equipment:**
Voltage waveform	Tektronix P5200 high-voltage differential probe
Current waveform	PEM CWT6R Rogowski current waveform transducer
Harmonic spectrum	HP 3562A signal analyzer
Efficiency, power loss	Yokogawa WT3000 power analyzer
Oscilloscope	Agilent MSO6034A
Capacitance, inductance and resistance	WK TMPRO 4230 LCR meter

power loss, and system efficiency. For example, the experimental setup for system efficiency measurements is illustrated in Fig. 5.2, with a Yokogawa WT3000 power analyzer connected to the input and output of *Prototype I*. The measurement equipment used during this project can be found in Table 5.2. Since all measurement results have been published and discussed in the references given above, only the most relevant results are included in this section.

With a modulation ratio of 0.96 and an active power output of 44 kW, a maximum total system efficieny of 93.2 % was measured [VI]. Fig. 5.5 shows the system efficiency as a function of the output line-to-line voltage. It can be noticed that SVM has a superior performance compared to SPWM especially at low-voltage conditions. Once the transformer current is sufficient to allow for non-resonant VSC commutations (for details about resonant VSC commutation, refer to [24]), the power losses are somewhat reduced, which shows in a slight step in system efficiency.

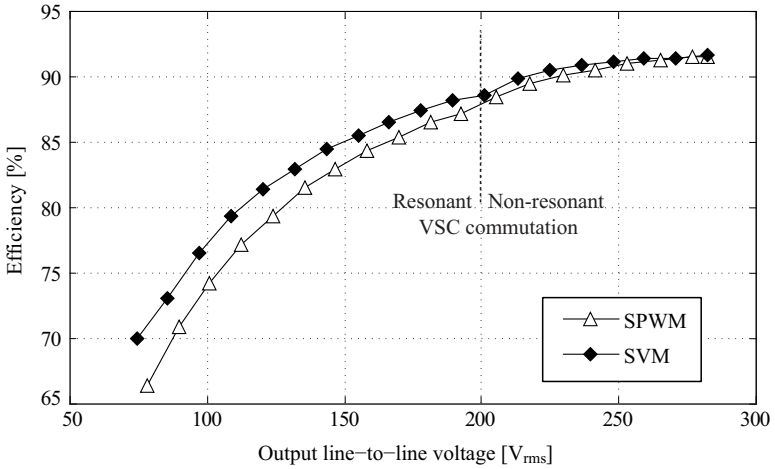

Figure 5.5: Measured total system efficiency of *Prototype I* as a function of the line-to-line voltage (with constant load resistance).

Fig. 5.6 shows a comparison of the RMS transformer current using either SPWM or SVM. The analytically calculated transformer currents show good agreement with the measurements, especially at high output voltages with non-resonant VSC commutations. The resonant current necessary for the VSC commuation at low load was not considered in the analytical calculations, which explains that the transformer current is somewhat underestimated for both SPWM and SVM at low output voltages. Comparing SVM with SPWM, the transformer current is considerably reduced at low output voltages due to the fact that SVM inherently maximizes the zero voltage vectors, during which no transformer current can flow. For higher output voltages, however, the transformer current converges for SVM and SPWM. This is due to the fact that the pulse patterns for SPWM and SVM are looking more and more alike at higher modulation ratios, where the zero voltage vectors are limited or entirely impossible.

5.2 Prototype II with thyristor-based cycloconverter

In order to experimentally verify the practical feasibility of an MCC system without cycloconverter turn-off capability, the 20 kVA *Prototype II* has been designed and manufactured, see Fig. 5.7. Compared to *Prototype I*, the IGBTs in the cycloconverter have been replaced with fast thyristors, see Fig. 5.8. This made a redesign of the cycloconverter main circuit and gate drive unit necessary, refer to Section 5.2.1. The MF transformer has also been replaced with a transformer adapted for the lower power rating and the 500 Hz operating frequency of *Prototype II*, refer to Section 5.2.2. All relevant parameters of *Prototype II* can be found in Table 5.3.

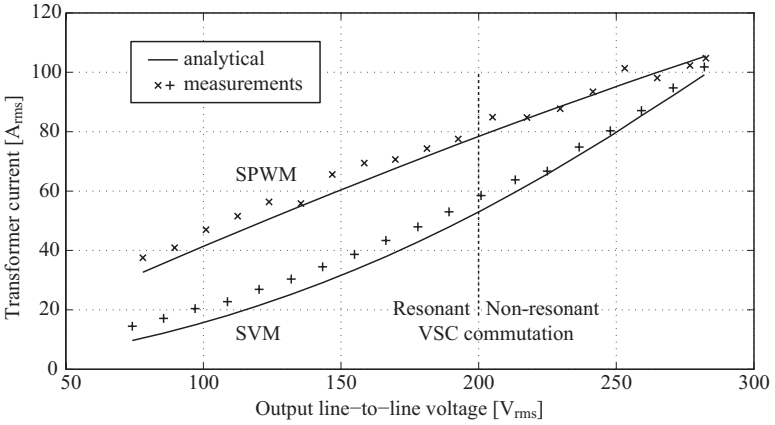

Figure 5.6: Measured and analytically calculated transformer current of *Prototype I* as a function of the line-to-line voltage (with constant load resistance).

Table 5.3: Parameters of *Prototype II*.

Rated power	20 kVA
DC-link voltage U_d	600 V
DC-link capacitance	2.9 mF
VSC snubber capacitance, per valve	0.22 μF
Transformer operating frequency	500 Hz
Transformer turns ratio	2:3
Transformer leakage inductance	179 μH
Transformer magnetizing inductance	60 mH
Cycloconverter RC-snubbers	25 Ω / 0.1 μF
AC-side filter inductors	24.4 mH

The VSC in *Prototype II* is the same as in *Prototype I*. Its design has been described in detail in [12, 24]. The VSC valves are implemented with standard IGBT modules BSM150GB120DLC from Eupec [50], designed for hard-switching applications. These IGBT modules, which are optimised for a low on-state voltage drop, have a blocking voltage of 1200 V and a rated current of 150 A. The modules are internally connected in a phase leg configuration and two modules are required for an H-bridge VSC. The 0.22 μF snubber capacitors of polypropylene type can be directly screwed onto the IGBT module terminals. Ten parallel-connected dry-film capacitors form the DC-link capacitance of 2.9 mF. A low-inductive connection between the IGBT modules and the DC-link capacitors is realized by a simple busbar consisting of two copper plates with a Mylar sheet in-between for insulation.

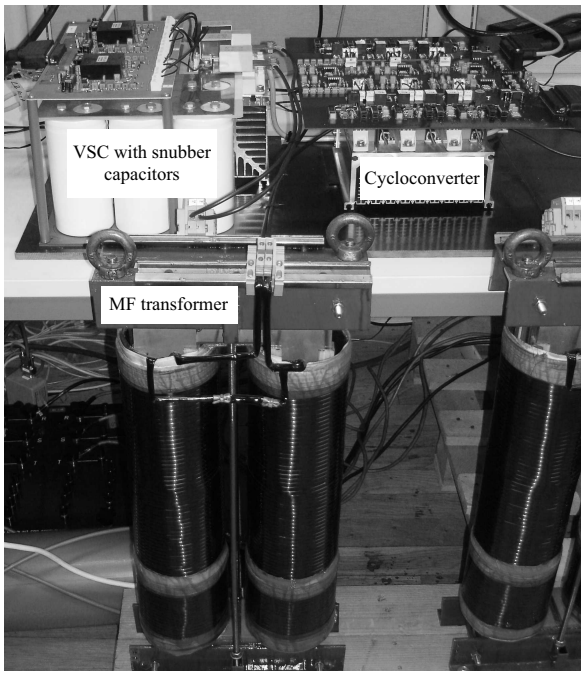

Figure 5.7: Photograph of *Prototype II*.

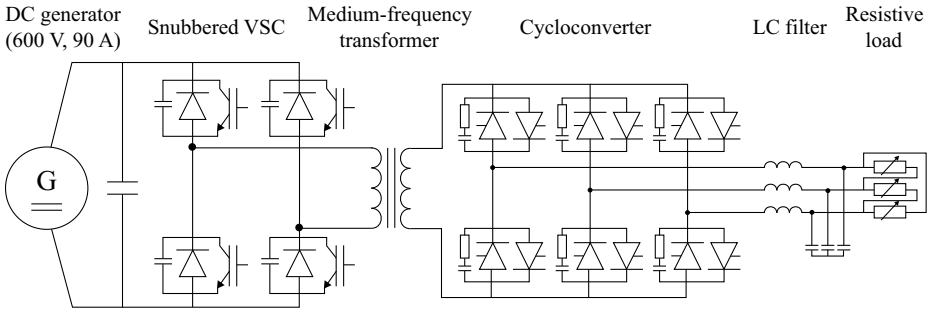

Figure 5.8: Schematic of *Prototype II*.

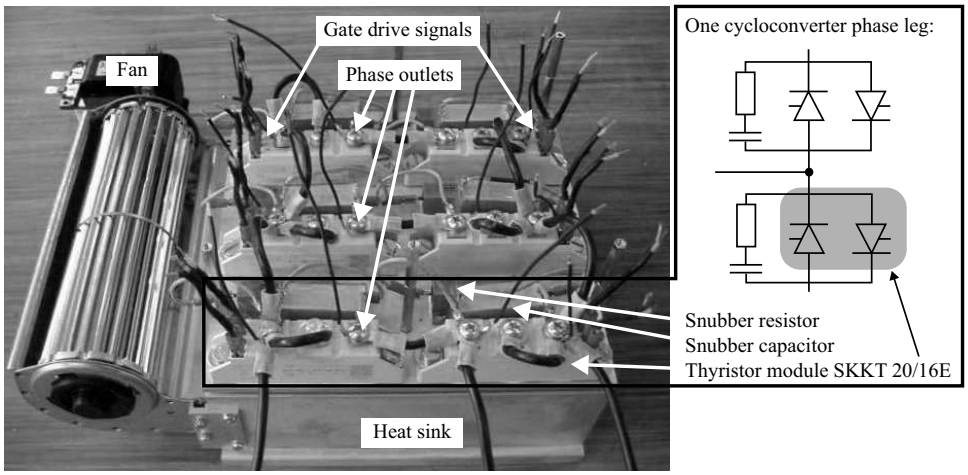

Figure 5.9: Main circuit of the thyristor-based cycloconverter.

5.2.1 Cycloconverter implementation

The cycloconverter, which is rated at approximately 20 kVA, is equipped with Semikron SKKT 20/16E dual thyristor modules [51]. These thyristor modules are rated for 1600 V repetitive peak reverse voltage and 40 A on-state current. Their specified turn-off time t_q is 80 μs. The thyristors are connected in such a way that one thyristor module forms a bidirectional valve, see Fig. 5.9. The cycloconverter valves are interconnected by cables, directly screwed onto the thyristor module terminals. No low-inductive connections are necessary, since the cycloconverter is anyway inductively coupled both on the input and output side.

The phenomenon of reverse current during the thyristor turn-off is well known. In this state, the thyristor has still a high amount of charge remaining and is able to conduct current in the reverse direction. Once the excess carriers in the thyristor no longer sustain the growing reverse current, it will start to fall towards zero, which results in an overvoltage due to the circuit inductance. This overvoltage has to be limited to an acceptable level with adequate RC-snubbers across the cycloconverter valves, see Fig. 5.9. References such as [31, 52–54] contain different considerations regarding the overvoltage limitation and the snubber circuit dimensioning. However, since the design of the thyristor snubber circuit depends on the operating conditions (junction temperature, commutation inductance, commutation voltage and current derivative during the turn-off) and on the thyristor component itself (waveform of the reverse recovery current and recovered charge) [53], measurements in a single-pulse test circuit have been performed in order to determine the optimum snubber parameters. Different thyristor snubber circuits and their capability to limit the overvoltage during thyristor turn-off have been evaluated. Finally, a snubber resistance of 25 Ω and a snubber capacitance of 0.1 μF was chosen. The snubber losses are independent of the snubber resistance, which can be chosen freely in order to limit the overvoltage. The choice of the snubber capacitance should be

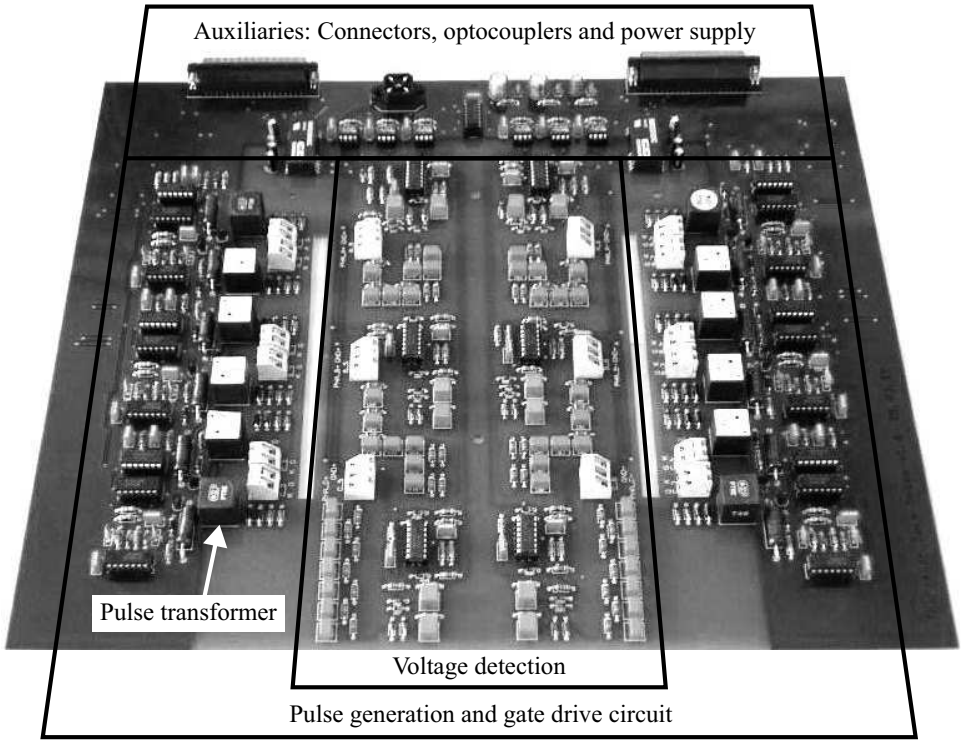

Figure 5.10: Gate drive unit for the thyristor-based cycloconverter.

large enough to avoid extensive overvoltages and small enough to limit the snubber losses. An RC-snubber is not ideal with respect to the snubber losses, since the snubber capacitor energy is fully dissipated in the snubber resistor during each commutation. Therefore, the mechanical design of the cycloconverter should ensure efficient cooling of the snubber resistor by direct contact with a heat sink, see Fig. 5.9. The arrangement should also be chosen in a way to limit unnecessary inductances in the cabling between the snubber circuits and the thyristors.

The main purpose of a gate drive unit for thyristors is to provide a gate current of the right amplitude and right duration at the right time. The gate drive unit for the cycloconverter in *Prototype II* shown in Fig. 5.10 was built up according to recommendations in [31, 55]. Since the thyristor is a current-controlled bipolar semiconductor, the gate drive unit is primarily a controlled current source. It is implemented as a pulse amplifier where the pulse signal turns on a MOSFET, which supplies an amplified gate current pulse to the thyristor through a pulse transformer [31]. In order to provide the desired current pulse shape to the thyristor gate, the pulse signal generation was implemented with an astable multivibrator. The first gate pulse should be large and long enough to reliably fire the thyristor, but not so long that it saturates the pulse transformer. Once triggered on, a thyristor continues to conduct even without any gate current. However, if the anode current falls below the holding current, a back-porch gate current is required to keep the

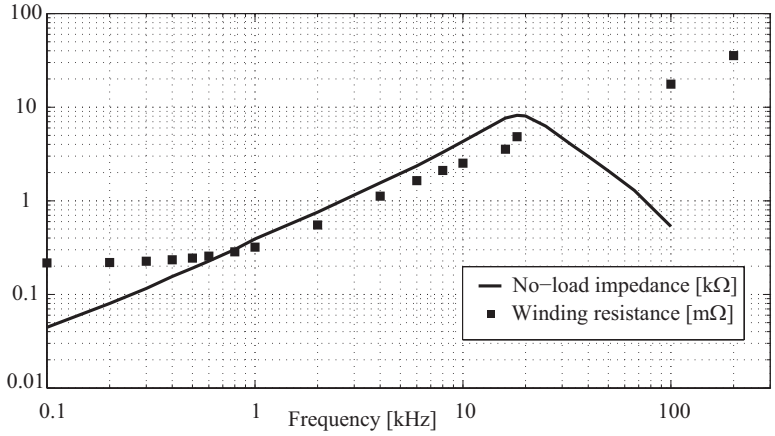

Figure 5.11: No-load impedance and winding resistance of the 500 Hz MF transformer in *Prototype II*.

thyristor in the on-state, which can be provided by picket fence current pulses [55]. These back-porch current pulses must be long enough to ensure that the thyristor is able to trigger at any time, at the same time as the repetition rate should be low enough to let the pulse transformer demagnetize between pulses. In addition to the gate drive function, circuitry for voltage detection and feedback of the switching state of the cycloconverter valves was integrated on the printed circuit board, see Fig. 5.10. The circuitry based on an RC voltage divider followed by a rapid comparator is described in [12]. It provides the control system with a digital signal telling whether the anode-cathode voltage is below or above a certain predefined level. This signal is used for determining when a commutation is finished.

5.2.2 Medium-frequency transformer implementation

The MF transformer design is adapted from a conventional 50 Hz sine-wave SLDC10 transformer from the manufacturer AQ Trafo AB [56], but with oriented steel sheets in order to reduce the no-load losses. The transformer windings are manufactured with regard to low leakage inductance, which is motivated by the demand for fast cycloconverter commutations. The flux density (down to 0.3 T) and the number of winding turns has also been adjusted in order to account for the increased operating frequency and the square-wave voltage that the transformer is exposed to. The characteristics of the transformer were measured with an LCR-meter and are shown in Fig. 5.11. The no-load impedance curve shows a parallel resonance between the winding capacitance and the magnetizing inductance around 18 kHz, which is confirmed by the measurement of the magnetizing inductance, which is in the range of 60 mH, see Table 5.3. Fig. 5.11 shows also the measured winding resistance at different frequencies. With increasing frequency, the winding resistance becomes more frequency dependent due to the skin and proximity effect.

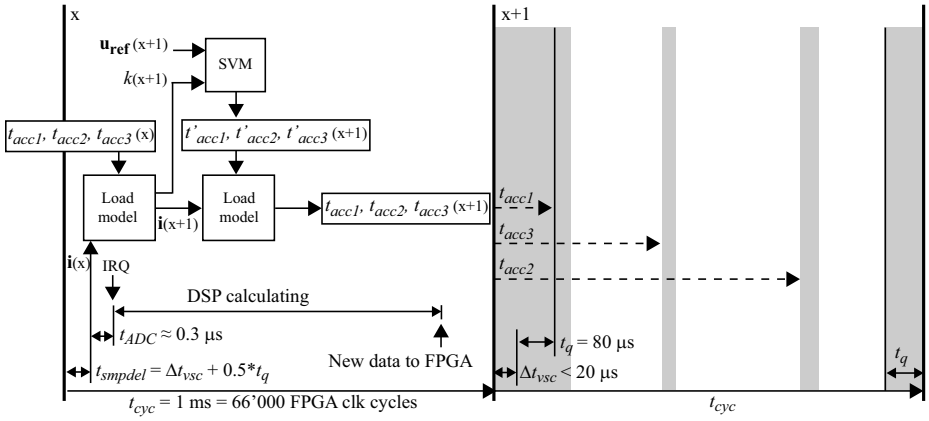

Figure 5.12: Implementation of current-clamping control strategy in *Prototype II*: Time diagram over two consecutive commutation cycles [VII].

5.2.3 Implementation of the current-clamping control strategy

The current-clamping control strategy proposed in Section 4.5 returns the control over the phase leg in which the current is changing sign by controlling the instant when the current clamping is released. However, such a control strategy is difficult to implement as it requires an accurate prediction of the current trajectory as well as the voltage vector during the current clamping [VII]. Fig 5.12 shows graphically how the current-clamping control strategy could be implemented in *Prototype II*.

At the beginning of a commutation cycle, the following information is available: The actual current vector $\mathbf{i}$(x), the phase leg commutation instants $t_{acc1}, t_{acc2}, t_{acc3}$(x) for the actual commutation cycle, and the reference voltage vector $\mathbf{u_{ref}}$(x+1) for the next commutation cycle. With the help of a load model embedded in the DSP, the current trajectory for the actual commutation cycle can be predicted, and thus the current sector k(x+1) at the beginning of the next commutation cycle. This is a prerequisite in order to calculate the preliminary phase leg commutation instants $t'_{acc1}, t'_{acc2}, t'_{acc3}$(x+1) with the standard SVM method [V]. With the help of the load model, the current vector trajectory during the next commutation cycle can be determined for the preliminary base vector sequence. In case of an imminent change of current sector, the base vector sequence can be altered according to the current-clamping control strategy, either to prevent a temporary current transition or to enhance a permanent current transition. In such a way, the modified switching instants for the cycloconverter phase leg commutations $t_{acc1}, t_{acc2}, t_{acc3}$(x+1) are calculated prior to the start of the commutation cycle. For more details about the implementation of the current-clamping control strategy, refer to [VII].

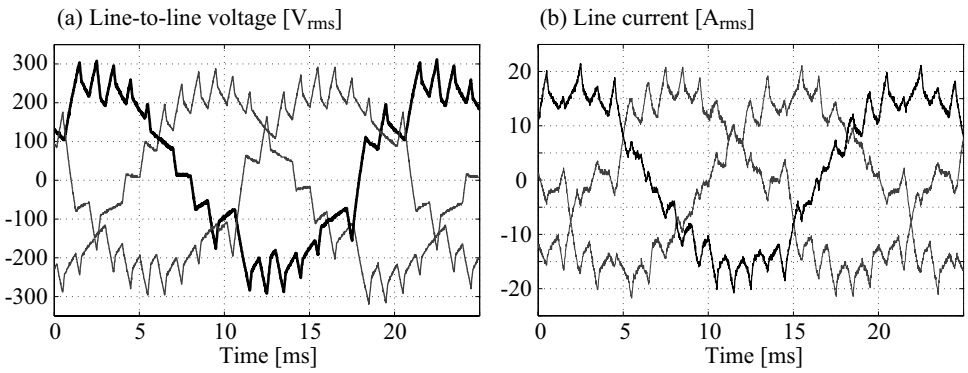

Figure 5.13: Measured waveforms from *Prototype II* operating at 20 % of rated load: (a) Line-to-line voltages, (b) Line currents.

5.2.4 Measurement results

This section presents and discusses measurement results from *Prototype II*. The measurements have been done at 20 % of rated load, i.e., at an output power of approximately 4 kVA. The presented results are preliminary, the current-clamping control strategy discussed above has not yet been implemented. Instead, a very rudimentary control strategy has been used, where either a current-sign reversal or a normal phase leg commutation is allowed during a commutation cycle. Therefore, the measurements should be considered as a first step towards the implementation of more advanced control strategies, showing the feasibility of a cycloconverter without turn-off capability in an MCC system. The measurements presented below indicate that only a software refinement remains to be done.

Fig. 5.13(a) shows the measured line-to-line output voltages. The relatively high voltage ripple is mainly due to the low switching frequency, but also due to the fact that the desired reference voltage vector could not be provided whenever one of the line currents was changing sign (due to the fact that the corresponding phase leg was not at all commutated). Fig. 5.13(b) shows the three line currents. A closer observation of the zero current crossings reveals some irregularities. Indeed, sometimes the same line current is changing sign under three consecutive commutation cycles, which is highly undesirable. This causes unnecessary distortion in the output voltage and confirms that a more advanced control strategy is necessary. Additional measurement results from *Prototype II* can be found in [VII].

The experimental results from *Prototype II* indicate that it is feasible to replace the IGBTs with fast thyristors in the cycloconverter of an MCC system. A cycloconverter without turn-off capability can be operated even with a very rudimentary control strategy. However, since there were some occasional commutation failures, an appropriate control strategy must ensure the proper turn-off of the thyristors in order to avoid accidental short-circuits. This is particularly important whenever

one of the line currents changes sign, which means that both anti-parallel thyristors in a valve had been turned on during the same commutation cycle.

5.3 Conclusions

The experimental activities covered the practical implementation of different modulation methods in a prototype converter system with an IGBT-based cycloconverter (refer to [VI]) and a second prototype converter system with a thyristor-based cycloconverter (refer to [VII]). Measurement results verified that both SVM for MCC systems and MCC systems without turn-off capability in the cycloconverter valves are practically feasible. However, only the proposed current-clamping control strategy is expected to be able to ensure a proper thyristor turn-off and at the same time provide the desired voltage output. Therefore, the practical implementation of the current-clamping control strategy is an obvious future activity, see Section 6.2.

The experimental activities have consciously been kept very general, thus not accounting for the special requirements of an MCC system in an offshore wind farm. This implies that aspects such as the distributed collection grid, the parallel operation of multiple cycloconverter sub-systems, etc. have not been considered. To integrate these aspects into the prototype converter systems is an important future activity, see Section 6.2.

6 Conclusions and future work

This chapter presents the conclusions of this thesis and suggests future work.

6.1 Conclusions

In this thesis, a mutually commutated soft-switching converter system is investigated, which provides a unique integrated solution for the wind turbine generator drive systems, the wind turbine interconnection, and the power conversion for HVDC transmission. This project has been focusing on finding solutions that enable an application of the MCC system in a wind farm.

Regarding the converter system itself, different carrier-based and space-vector oriented methods suitable for the modulation of the output voltages have been investigated. An analogy between space vector modulation and quasi-discontinuous pulse width modulation has been established, which works for any load angle. In addition, a modulation strategy for thyristor-based cycloconverters has been developed, which can provide the desired output voltage during every single commutation cycle despite the lack of turn-off capability of the thyristors. The feasibility of different modulation strategies for MCC systems has been verified on a down-scaled 40 kVA prototype converter system with both IGBT- and thyristor-based cycloconverters.

Regarding the application of an MCC system in a wind farm, different system aspects have been investigated. Special attention is paid to the design of the MF collection grid, including the magnetical, electrical, and thermal design of the MF distribution and transmission transformers. In order to limit transient overvoltages on the collection grid, which are caused by interference between system resonances and low-order voltage harmonics, the voltage slope during the VSC commutation should be kept within a certain limit depending on the layout of the collection grid. A possible solution is the use of thyristor-controlled snubber capacitors, which can control the duration of the VSC commutation independent of the actual power generation. At the same time, thyristor-controlled snubber capacitors solve the problem with the VSC commutation during low power generation.

In this thesis, it is shown that both the conversion losses and the initial costs in a wind farm based on an MCC system may considerably be decreased, thus reducing the energy generation costs. However, design proposals of feasible wind farm layouts

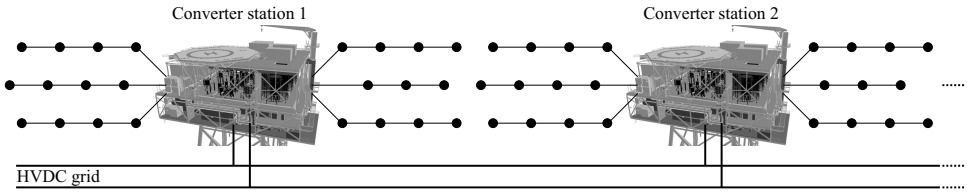

Figure 6.1: Proposal of a modular approach of a scalable wind farm layout.

for large wind farms show that some of the advantages of the mutual commutation are countervailed by disadvantages of a distributed collection grid. Therefore, larger wind farms should favorably be divided into smaller sections, each with an offshore converter platform that is connected to an HVDC grid, refer to Fig. 6.1. Such a solution would not only significantly reduce the size of the collection grids and the associated problems with transient overvoltages, but also somewhat reduce the collection grid losses due to the higher voltage level on the DC grid. In addition, such a modular approach would increase the reliability and allow to scale a wind farm ad libitum.

6.2 Future work

During the progess of work, several suggestions for future work have come up:

Implementation of current-clamping control strategy: The feasibility of a MCC system with a cycloconverter equipped with thyristors has been experimentally verified [VII]. The current-clamping control strategy, which is an original contribution proposed in [V], seems to have superior properties regarding the maximum possible modulation ratio as well as the harmonic distortion in the output voltage. Therefore, the practical implementation of the current-clamping control strategy is an obvious future activity.

The main challenge regarding the implementation of the current-clamping control strategy is the requirement for accurate current measurement and current prediction. In order to be able to precisely predict the current vector trajectory for the two subsequent commutation cycles, an accurate wind turbine generator model is necessary. In practice, oversampling the current measurement could increase the accuracy of the current prediction and reduce the computational time of the DSP.

Experimental setup: The prototype converter could be extended by a second subsystem (MF transformer and cycloconverter), representing a second wind turbine connected to the collection grid. Such an arrangement would enable investigations about the interaction between different subsystems and reveal possible problems.

Another improvement of the experimental setup would be to replace the resistive load by a squirrel-cage induction generator driven by a motor. This would not only change the direction of power flow as it is the case in a real wind farm, but also allow the verification of the wind turbine generator model in the current predictor of the current-clamping control strategy.

Filter design: In order to limit transient overvoltages and damp voltage ringing on the MF collection grid, an input filter could be installed in every wind turbine. Such a filter should have a characteristic that is resistive at high frequencies and capacitive at low frequencies. A possible solution could be a second order shunt filter, which fulfills the filtering requirements independent of the cable length [57].

Depending on the modulation method of the cycloconverter, the harmonic distortion in the output voltage causes additional losses in the wind turbine generator. Therefore, it should be investigated to what extent a cycloconverter output filter could reduce these harmonic losses. The required ratings of the elements of such a filter must also be determined in order to predict the additional cost for the filter.

Failure conditions: Different failures can disrupt the operation of a wind farm: Trip, fault or overspeed of a wind turbine generator, converter commutation faults, cable faults, transformer faults, short circuits, etc. Nevertheless, the control and protection system of a wind farm is required to comply with current network connection regulations, such as fault ride-through and black-start capability requirements. Even though the proposed topology does not differ significantly from conventional VSC-based HVDC transmission systems, it should be investigated how exactly different failure conditions could be handled best.

A natural first step towards the implementation of the proposed topology would be to focus on a compact MCC system as shown in Fig. 2.6. Without affecting the surrounding system, this would permit to simply replace the three-phase VSC and line-frequency transformer in a conventional converter station with a single-phase VSC, an MF transformer, and a cycloconverter. However, the overall advantages of a compact MCC system should first be investigated in order to justify such an approach.

References

[1] Vindforsk. `http://www.vindenergi.org`.

[2] Elforsk. `http://www.elforsk.se`.

[3] Swedish Energy Agency. `http://www.swedishenergyagency.se`.

[4] J. Kreusel, "The future is now - Linking up the worlds largest offshore windfarm area with HVDC transmission." ABB Review 4/2008.

[5] "Pure Power - Wind Energy Scenarios up to 2030." European Wind Energy Association, March 2008.

[6] K. Eriksson, C. Liljegren, and K. Sœbrink, "HVDC Light Experiences Applicable for Power Transmission from Offshore Wind Power Parks", in *42nd AIAA Aerospace Sciences Meeting and Exhibit*, no. AIAA-2004-1010, Reno, Nevada, Published by the American Institute of Aeronautics, January 5-8, 2004.

[7] A. Skytt, P. Holmberg, and L. Juhlin, "HVDC Light for Connection of Wind Farms", in *Second International Workshop on Transmission Networks for Offshore Wind Farms*, Royal Institute of Technology, Stockholm, Sweden, March 29-30, 2001.

[8] T. Ackermann, ed., *Wind Power in Power Systems*. John Wiley & Sons, Ltd, 2005.

[9] K. Sœbrink, P. Sœrensen, E. Joncquel, and D. Woodford, "Feasibility study regarding integration of the Læsø Syd 160 MW wind farm using VSC transmission", in *CIGRE SC14 Colloquium*, Three Gorges Dam Site, VR China, August 31, 2001.

[10] N. Kirby, L. Xu, M. Luckett, and W. Siepmann, "HVDC transmission for large offshore wind farms", in *Power Engineering Journal*, vol. 16, pp. 135–141, June 2002. Issue 3.

[11] S. Norrga, "A Novel Soft-switched Bidirectional Isolated AC/DC Converter", in *Procedings of the Conference on Power Conversion and Intelligent Motion, PCIM '02*, Nuremberg, Germany, May 2002.

[12] S. Norrga, "An Experimental Study of a Soft-switched Isolated AC/DC Converter without Auxiliary Circuit", in *Proceedings of the 35th IEEE Power Electronics Specialists Conference, PESC '04*, Aachen, Germany, June 2004.

[13] Z. Shuang, "Mutually commutated converter equipped with thyristor-based cycloconverter", Master's thesis, Chalmers University of Technology, Gothenburg, Sweden, 2008.

[14] M. Kuschke, "Practical implementation of a cycloconverter in a soft-switching isolated AC/DC converter", tech. rep., Royal Institute of Technology, Stockholm, Sweden, 2007.

[15] L. Nian, "Transients in the Collection Grid of a novel Wind Farm Topology", Master's thesis, Royal Institute of Technology, Stockholm, Sweden, April 2009.

[16] P. Cartwright, L. Xu, and C. Sasse, "Grid Integration of Large Offshore Wind Farms Using Hybrid HVDC Transmission", in *Proceedings of the Nordic Wind Power Conference*, Gothenburg, Sweden, March 1-2, 2004.

[17] ABB. `http://www.abb.com`.

[18] U. Axelsson, A. Holm, C. Liljegren, K. Eriksson, and L. Weimers, "Gotland HVDC Light Transmission - World's First Commercial Small Scale DC Transmission", in *Proceedings of the CIRED conference*, Nice, France, May 1999.

[19] B. Andersen, L. Xu, P. Horton, and P. Cartwright, "Topologies for VSC transmission", in *Power Engineering Journal*, vol. 16, pp. 142–150, June 2002. Issue 3.

[20] R. Marquardt and A. Lesnicar, "New Concept for High Voltage - Modular Multilevel Converter", in *Proceedings of the 35th IEEE Power Electronics Specialists Conference, PESC '04*, Aachen, Germany, June 2004.

[21] A. Lesnicar and R. Marquardt, "A new modular voltage source inverter topology", in *Proceedings of the 10th European Conference on Power Electronics and Applications, EPE '03*, Toulouse, France, September 2003.

[22] B.-T. Ooi, "Research Opportunities in High Power Electronics", in *International Conference on Power Electronics and Drives Systems, PEDS*, vol. 1, pp. 17 – 22, 2005.

[23] Siemens. `http://www.ptd.siemens.de`.

[24] S. Norrga, *On Soft-Switching Isolated AC/DC Converters without Auxiliary Circuit*. PhD thesis, Department of Electrical Engineering, Royal Institute of Technology, Stockholm, Sweden, 2005.

[25] K. Søbrink, D. Woodford, R. Belhomme, and E. Joncquel, "AC Cable versus DC Cable Transmission for Offshore Wind Farms, a Study Case", in *Fourth International Workshop on Large-Scale Integration of Wind Power and Transmission Networks for Offshore Wind Farms*, Billund, Denmark, October 20-21, 2003.

[26] P. Christiansen, K. Jørgensen, and A. Sørensen, "Grid Connection and Remote Control for the Horns Rev 150 MW Offshore Wind Farm in Denmark", in *EPSRC Offshore Wind Energy Network Workshop on Electrical Design of Offshore Wind Installations*, Oxfordshire, UK, November 7, 2000.

[27] U. Axelsson, A. Holm, C. Liljegren, M. Åberg, K. Eriksson, and O. Tollerz, "The Gotland HVDC Light Project - Experiences from Trial and Commercial Operation", in *Proceedings of the CIRED conference*, Amsterdam, The Netherlands, June 18-21, 2001.

[28] S. Green, "HVDC Systems Gotland: the HVDC pioneer." in Power Engineering International, July 2004.

[29] "Tjæreborg HVDC Light project: Enge - Tjæreborg, Denmark." Pamphlet no POW-0022, `http://www.abb.com/powersystems`.

[30] K. Søbrink, P. Sørensen, P. Christensen, N. Andersen, K. Eriksson, and P. Holmberg, "DC Feeder for Connection of a Wind Farm", in *CIGRE Symposium*, Kuala Lumpur, Malaysia, September 1999.

[31] N. Mohan, T. Undeland, and W. Robbins, *Power Electronics - Converters, Applications, and Design*. John Wiley & Sons, Inc., second edition ed., 1995.

[32] *PSCAD - User's guide*, version 4.0.2, second printing ed., July 18, 2003. `http://www.pscad.com`.

[33] L. Liljestrand, A. Sannino, H. Breder, and S.Johansson, "Transients in Collection Grids of Large Offshore Wind Parks", in *Proceedings of the Nordic Wind Power Conference*, Espoo, Finland, May 2006.

[34] T. Abdulahovic, "Analysis of High-Frequency Electrical Transients in Offshore Wind Parks." Licenciate thesis, Department of Energy and Environment, Chalmers University of Technology, Göteborg, Sweden, 2009.

[35] R. Raad, T. Henriksen, H. Raphael, and A. Hadler-Jacobsen, "Converter-Fed Subsea Motor Drives", *IEEE Transactions on Industry Applications*, vol. 32, pp. 1069–1079, September-October 1996.

[36] A. von Jouanne and P. Enjeti, "Design Considerations for an Inverter Output Filter to Mitigate the Effects of Long Motor Leads in ASD Applications", in *IEEE Transactions of Industry Applications*, vol. 33, September/October 1997.

[37] ABB, "XLPE Cable Systems - User's guide." rev. 2, `http://www.abb.com/cables`.

[38] T. Kjellqvist, S. Norrga, and S. Östlund, "Design Considerations for a Medium Frequency Transformer in a Line Side Power Conversion System", in *Proceedings of the 35th Annual IEEE Power Electronics Specialists Conference, PESC '04*, Aachen, Germany, June 2004.

[39] M. Popov, *Switching Three-Phase Distribution Transformers with a Vacuum Circuit Breaker - Analysis of Overvoltages and the Protection of Equipment*. PhD thesis, Delft University of Technology, November 2002.

[40] S. Bowes and B. Bird, "Novel approach to the analysis and synthesis of modulation processes in power converters", *Proc. IEE*, vol. 122, pp. 507–513, May 1975.

[41] S. Bowes, "New sinusoidal pulsewidth-modulated invertor", *Proc. IEE*, vol. 122, pp. 1279–1285, November 1975.

[42] M. Matsui, M. Nagai, M. Mochizuki, and A. Nabae, "High-Frequency Link DC/AC Converter with Suppressed Voltage Clamp Circuits - Naturally Commutated Phase Angle Control with Self Turn-Off Devices", *IEEE Transactions on Industry Applications*, vol. 32, pp. 293–300, March/April 1996.

[43] M. Matsui, T. Kitano, S. Ohba, and D. Xu, "New space vector modulation scheme based high-frequency linksoft-switching converter for AC system line interface", in *Proceedings of the Power Conversion Conference, PCC '02*, vol. 2, Osaka, Japan, pp. 478–485, April 2002.

[44] S. Norrga, "Modulation Strategies for Mutually Commutated Isolated Three-Phase Converter Systems", in *Proceedings of the 36th Annual Power Electronics Specialists Conference, PESC '05*, Recife, Brazil, June 2005.

[45] L. Malesani, P. Tomasin, and V. Toigo, "Space Vector Control and Current Harmonics in Quasi-Resonant Soft-Switching PWM Conversion", *IEEE Transactions on Industry Applications*, vol. 32, pp. 269–278, March/April 1996.

[46] D. G. Holmes and T. A. Lipo, eds., *Pulse Width Modulation for Power Converters, Principles and Practice*. IEEE Press, John Wiley & Sons, Inc., 2003.

[47] F. Iturriz and P. Ladoux, "Phase-controlled multilevel converters based on dual structureassociations", *IEEE Transactions on Power Electronics*, vol. 15, pp. 92–102, January 2000.

[48] J. Holtz and B. Beyer, "The Trajectory Tracking Approach - A New Method for Minimum Distortion PWM in Dynamic High-Power Drives", *IEEE Transactions on Industry Applications*, vol. 30, pp. 1048–1057, July-August 1994.

[49] J. Holtz and N. Oikonomou, "Synchronous Optimal Pulsewidth Modulation and Stator Flux Trajectory Control for Medium-Voltage Drives", *IEEE Transactions on Industry Applications*, vol. 43, pp. 600–608, March-April 2007.

[50] Eupec/Infineon Power Semiconductors. `http://www.eupec.com`.

[51] Semikron. `http://www.semikron.com`.

[52] M. O. Popescu, D. Nistor, and C. Popescu, "R-C Snubber for Thyristor Turn-off / a New Approach", in *Proceedings of the IEEE International Symposium on Industrial Electronics, ISIE '96*, vol. 1, pp. 505–507, June 1996.

[53] ABB, "Design of RC Snubbers for Phase Control Applications." Application Note, 2001. `http://www.abb.com`.

[54] Fairchild Semiconductor, "RC Snubber Networks for Thyristor Power Control and Transient Suppression." Application Note AN-3008, 2002. `http://www.fairchildsemi.com`.

[55] B. Backlund, A. Schweizer, J. Waldmeyer, and E. Carroll, "Gate-drive Recommendations for Phase Control Thyristors." Phase Control Thyristors Application Note, September 2002. `http://www.abb.com`.

[56] AQ Trafo AB. `http://www.aqg.se/trafo`.

[57] A. von Jouanne, D. Rendusara, P. Enjeti, and J. Gray, "Filtering techniques to minimize the effect of long motor leads on PWM inverter-fed AC motor drive systems", *IEEE Transactions on Industry Applications*, vol. 32, pp. 919 – 926, July-August 1996.

List of acronyms

ABB	Asea Brown Boveri
AC	Alternating Current
ADC	Analog-to-Digital Converter
AEP	Annual Energy Production
ASG	Adjustable Speed Generator
B2B	Back-to-back VSC
DC	Direct Current
DFIG	Doubly-Fed Induction Generator
DSP	Digital Signal Processor
FPGA	Field-Programmable Gate Array
FSM	Finite State Machine
HVAC	High-Voltage Alternating Current
HVDC	High-Voltage Direct Current
IEC	International Electrotechnical Commission
IGBT	Insulated Gate Bipolar Transistor
KTH	Kungliga Tekniska Högskolan (Royal Institute of Technology)
LCC	Line-Commutated Converter
MCC	Mutually Commutated Converter
MF	Medium-Frequency
M^2LC	Modular MultiLevel Converter
PC	Personal Computer
PSCAD	Power Systems Computer Aided Design
PWM	Pulse Width Modulation
QDPWM	Quasi-Discontinuous Pulse Width Modulation
RMS	Root Mean Square
SPWM	Sinusoidal Pulse Width Modulation
STATCOM	STATic COMpensator
SVC	Static VAr Compensator
SVM	Space Vector Modulation
THD	Total Harmonic Distortion
TSO	Transmission System Operator
VSC	Voltage Source Converter
XLPE	Cross-linked Polyethylene